Coordination Chemistry Reviews 255 (2011) 1713–1732

Contents lists available at ScienceDirect

Coordination Chemistry Reviews

journal homepage: www.elsevier.com/locate/ccr

Review

Tricyanometalate molecular chemistry: A type of versatile building blocks for the construction of cyano-bridged molecular architectures

Shi Wang[a,b,*], Xue-Hua Ding[a], Jing-Lin Zuo[b], Xiao-Zeng You[b], Wei Huang[a,**]

[a] Key Laboratory of Organic Electronics & Information Displays (KLOEID) and Institute of Advanced Materials (IAM), Nanjing University of Posts & Telecommunications, Nanjing 210046, China
[b] State Key Laboratory of Coordination Chemistry, Nanjing University, Nanjing 210093, China

Contents

ARTICLE INFO

Article history:
Received 19 November 2010
Accepted 31 January 2011
Available online 5 March 2011

Keywords:
Cyanocomplexes
Crystal structures
Magnetic properties
Clusters
Single-molecule magnets
Single-chain magnets

ABSTRACT

Cyano-bridged molecule-based magnetic materials with reduced dimensionality, such as single-molecule magnets (SMMs) and single-chain magnets (SCMs), have attracted great research interest during the last decade. Among the cyano-based molecular precursors with ample coordinating capability, we note the ability of the tricyanometalate to link various metal ions lead to a wide diversity of structural architectures ranging from discrete polynuclear complexes to various one-dimensional (1D) assemblies. Some of them are promising cyano-bridged SMMs and SCMs. The use of capping tridentate organic ligands results in a number of clusters containing di-, tri-, tetra-, penta-, hexa-, octa-, fourteen-nuclear and various 1D metal-cyanide molecular architectures. Here we review the structural topologies of these complexes and their related magnetic properties, highlight typical examples, and point out the main possible directions that remain to be developed in this field. From the crystal engineering point of view, the compounds reviewed here should provide useful information for further design and investigation on this elusive class of cyano-bridged SMMs and SCMs.

1. Introduction

Cyano-bridged infinite systems (or Prussian blue analogues) have been subject of intensive research during the last two decades [1–4]. The variety in their structures associated with their interesting functional properties, such as molecular sieves [5], hosts for small molecules and ions [6], catalysts for the production of ether polyols or polycarbonates [7], room temperature magnets [8], electrochemically tunable magnets [9], photo-magnetic materials [10] and magneto-optical effect [11], make them suitable compounds for the design of new materials.

* Corresponding author at: Key Laboratory of Organic Electronics & Information Displays (KLOEID) and Institute of Advanced Materials (IAM), Nanjing University of Posts & Telecommunications, Wenyuan Road 9, Nanjing, Jiangsu 210046, China. Tel.: +86 25 85866396; fax: +86 25 85866396.
** Corresponding author. Tel.: +86 25 85866396; fax: +86 25 85866396.
E-mail addresses: iamswang@njupt.edu.cn (S. Wang), wei-huang@njupt.edu.cn (W. Huang).

0010-8545/$ – see front matter © 2011 Elsevier B.V. All rights reserved.
doi:10.1016/j.ccr.2011.01.057

Cyano-bridged molecule-based magnetic materials with reduced dimensionality, such as single-molecule magnets (SMMs) [12] and single-chain magnets (SCMs) [13–16], have attracted great research interest because they can retain information in a single molecule or in a one-dimensional (1D) compound rather than in a magnetic particle or array of particles [17] and can potentially be used in quantum computers for information storage [18,19]. Important to the future of the field of SMMs and SCMs is the development of new synthetic schemes that can yield compounds with a large spin, anisotropy and/or strong magnetic coupling. Metal-cyanide systems offer a great advantage for achieving such control, through the substitution of various metal ions into a given structure type. Moreover, the nature of the magnetic exchange coupling between different metal ions in the resulting compounds is readily predicted [20].

One synthetic approach to attain discrete polynuclear and 1D systems is to utilize molecular precursors with ample coordinating capability, for instance, $[M_A(CN)_x]^{n-}$ ($x = 6$, 8), and their counterparts having specific vacant sites or labile leaving ligands, $[M_BL_xL'_y]^{m+}$ (L = polydentate ligand, L′ = labile group) [3,4,21]. This approach was first demonstrated by Mallah and Murray on the control of the nuclearity in making cyano-bridged heptanuclear complexes [22]. In this situation, the denticity of the polydentate ligand becomes a determining factor for molecular dimensionality and molecular structure. Recently, a more efficient strategy in which capped cyano-coordinated building units $[LM_A(CN)_x]^{n-}$ ($x = 2$ dicyano, 3 tricyano, 4 tetracyano; $n = 0$, 1, 2) were employed as synthons to achieve low-dimensional magnetic complexes has been successfully devised [13,23–25]. These building blocks containing the paramagnetic 3d metal ions have been extensively explored, giving diverse structural motifs spanning from clusters to 1D and two-dimensional (2D) assemblies. Among them, we note the ability of the tricyanometalate to link various metal ions lead to a wide diversity of structural architectures ranging from discrete polynuclear complexes to various 1D assemblies. Some of them are promising cyano-bridged SMMs and SCMs. When L is a tridentate ligand, the control of the stereochemistry of the precursor, $[LM_A(CN)_3]$, is important because the three cyanide groups can have a *fac* or *mer* arrangement depending on the use of specific ligand. For example, facially coordinated tripodal ligands (Cp = cyclopentadiene) were introduced to replace three of these cyanides which block one face of the octahedron [25]. Polymerization could be inhibited, and a family of cages with a box-like architecture results.

Beltran and Long have reported the use of neutral tricyanometalate precursor *fac*-$[LM_A(CN)_3]$ in the design of metal-cyanide cluster magnets: *fac*-$[LM_A(CN)_3] + [M_BL_xL'_y]^{m+}$ [23]. In an effort to extend this chemistry, we and other research groups have chosen to employ $[LM_A(CN)_3]^-$ as the precursor compounds: $[LM_A(CN)_3]^- + [M_BL_xL'_y]^{m+}$. In contrast to the neutral *fac*-$[LM_A(CN)_3]$, these monoanionic complexes can have a *fac* or *mer* arrangement and are negatively charged which help alleviate the build-up of excessive charge in clusters and chains, make the synthesis of the target compounds easy. Thus, $[LM_A(CN)_3]^-$ had been anticipated to direct the formation of new cyano-bridged compounds with various interesting structures and magnetic properties. Indeed, the use of capping tridentate organic ligands results in a number of clusters containing di-, tri-, tetra-, penta-, hexa-, octa-, fourteen-nuclear clusters and various 1D molecular architectures. Thus, this review is focused on the structural topologies of these complexes and their magnetic properties.

2. Tricyanometalate precursors

After the report by Julve's group on the first anionic tricyanometalate precursor *fac*-$[TpFe(CN)_3]^-$ (Tp = hydrotris(pyrazolyl)borate) [26], interest in making different anionic $[LM_A(CN)_3]^-$ building block having various ligands and paramagnetic metal centers has been long-standing in a few groups and several anionic tricyanometalate precursors have been published: (i) paramagnetic *fac*-$[LM_A(CN)_3]^-$ ($M_A = Fe^{III}$, L = Tp [26], hydrotris(3,5-dimethylpyrazolyl)borate (Tp*) [27], tetrakis(pyrazolyl)borate (pzTp) [28], tris(pyrazolyl)phenylborate (phTp), methyltris(pyrazolyl)borate (MeTp), 2-methylpropyltris(pyrazolyl)borate (*i*BuTp) [29], Cr^{III}, L = Tp [30]; *fac*-$[LM_A(CN)_3]^-$ ($M_A = V^{III}$, L = Tp* [31]) and *mer*-$[LM_A(CN)_3]^-$ ($M_A = Fe^{III}$, L = bis(2-pyridylcarbonyl)amide (bpca) [32]), 8-(pyrazine-2-carboxamido)quinoline anion (pzcq) [33], 8-(5-methylpyrazine-2-carboxamido)quinoline anion (mpzcq) [34], 2,3,5,6-tetrakis(2-pyridyl)pyrazine (tppz) [35], 8-(2-quinolinecarboxamido)quinoline anion (qcq) [36]; (ii) diamagnetic *fac*- and *mer*-$[LM_A(CN)_3]^-$ ($M_A = Fe^{II}$, L = tppz [35], bis(2-pyridylmethyl)amine (2-DPA) [37]); *fac*-$[LM_A(CN)_3]^{2-}$ ($M_A = Fe^{II}$, L = Tp* [27], tris(pyrazolyl)methane sulfonate (Tpms) [38]). In general, the preparation of these anionic precursors can be achieved by the reaction of the $Fe^{II}(L)_2$ (L = Tp, Tp*) and KCN in a 1:3 stoichiometry to make the corresponding $[LFe^{II}(CN)_3]^{2-}$, followed by the oxidation of the $[LFe^{II}(CN)_3]^{2-}$ to the final $[LFe^{III}(CN)_3]^-$.

Crystallographic investigations have been reported for most of the above mentioned complexes. The molecular structure consists of the *fac*-$[LM_A(CN)_3]^{-/2-}$ or *mer*-$[LM_A(CN)_3]^{-/2-}$ anion (Fig. 1), the uncoordinated (tetraphenylphosphonium) PPh_4^+ (or tetrabutylammonium cation (NBu_4^+), tetraethylammonium cation (NEt_4^+) and K^+) counter cations, and sometimes the crystallization solvent molecules. The Fe/V/Cr atom has a slightly distorted octahedral coordination geometry, its symmetry either being close to C_{3v} for the *fac*-symmetry or being close to C_{2v} for *mer*-symmetry. Good agreement is observed between the Fe–C (1.910(6)–1.929(7) Å) and Fe–N (1.970(4)–1.987(4) Å) distances and those reported for other mononuclear low-spin (LS) iron(III) compounds. The magnetic moment at room temperature ($\mu_{eff} = 2.4\mu_B$) demonstrates the LS character of the iron(III).

The IR spectra of these precursors show a middle strong band between 2000 and 2200 cm^{-1} that correspond to the cyanide stretching frequency.

3. Multinuclear assemblies

3.1. Dinuclear cyano-bridged complexes

Three kinds of dinuclear cyano-bridged complexes based on the anionic tricyanometalate precursor, $[LFe(CN)_3]^-$, have been reported: (i) Fe^{III}–Mn^{II} dimers: $[Fe(pzcq)(CN)_3][Mn(phen)_2(X)]\cdot MeOH$ (phen = 1,10-phenanthroline; X = Cl or Br) and $[Fe(mpzcq)(CN)_3][Mn(phen)_2(Cl)]\cdot MeOH$ [39]; (ii) Fe^{III}–Cu^{II} dimers: $[(Tp)Fe^{III}(CN)_3Cu^{II}(bipy)_2]\cdot ClO_4\cdot CH_3OH$ (bipy = 2,2′-bipyridine) [40] and *fac*-$\{[Fe^{III}(pzTp)(CN)_2(\mu\text{-}CN)]Cu^{II}(TPyA)\}\cdot Et_2O\cdot ClO_4$ (TPyA = Tris(2-pyridylmethyl)amine) [41]; (iii) Fe^{III}–Mn^{III} dimers: $[Mn(D,L\text{-}Lb)(DMF)(Tp)Fe(CN)_3]\cdot(H_2O)_6$ (Lb = cis-N,N′-(2-hydroxybenzylidene)-1,2,2-trimethylcyclopenta-1,3-diamine; DMF = dimethylformamide) [42], $[(Tp)Fe(CN)_3][Mn(1\text{-napen})(H_2O)]\cdot MeCN\cdot 4H_2O$ (1-napen = N,N′-ethylene-bis(2-hydroxy-1-naphthylideneiminato) dianion), $[(Tp)Fe(CN)_3][Mn(5\text{-Clsalen})(H_2O)]$ (5-Clsalen = N,N′-(trans-1,2-cyclohexanediyl-ethylene) bis(5-chlorosalicylideneiminato) dianion), $[(Tp)Fe(CN)_3][Mn(2\text{-acnapen})(MeOH)]\cdot MeOH$ (2-acnapen = N,N′-ethylene bis(1-hydroxy-2-acetonaphthylideneiminato) dianion), $[(Tp)Fe(CN)_3][Mn(3\text{-MeOsalen})(H_2O)]$ (3-MeOsalen = N,N′-ethylenebis(3-methoxysalicylideneiminato) dianion) [43], $[Fe(mpzcq)(CN)_3][Mn(salen)(H_2O)]\cdot H_2O$ (salen = N,N′-

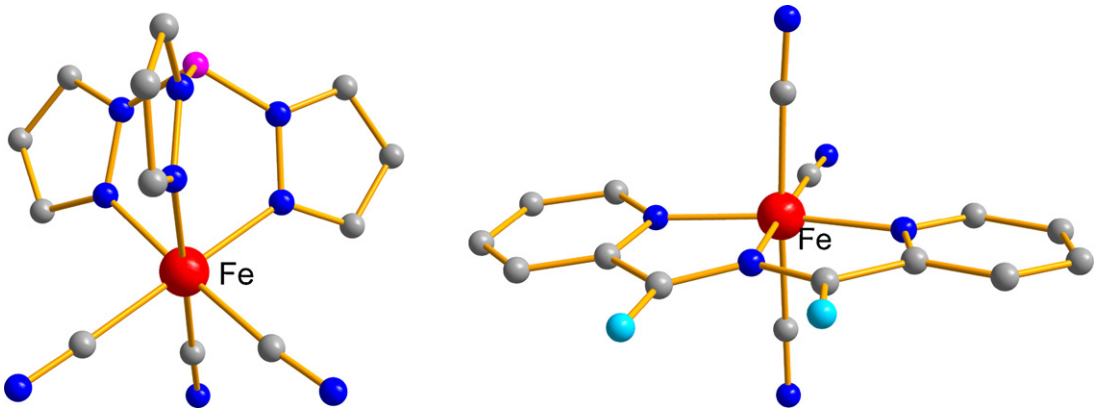

Fig. 1. View of the molecular structure of the anionic tricyanometalate precursors *fac*-$[LM_A(CN)_3]^-$ (L = Tp) (left) and *mer*-$[LM_A(CN)_3]^-$ (L = bpca) (right) [26,32].

ethylenebis(salicylidineiminato) dianion) [34] and $[Fe(qcq)(CN)_3][Mn(3\text{-}MeOsalen)(H_2O)]\cdot 2H_2O$ [36]. Typically, the polycrystalline materials are obtained by slow evaporation of the reaction solutions at room temperature for a few days. The IR spectra of these complexes show a group of narrow and strong bands between 2110 and 2150 cm^{-1} that correspond to the $\upsilon_{C\equiv N}$ stretching frequency. The shift of $\upsilon_{C\equiv N}$ to higher wave number as compared to that of $[LFe(CN)_3]^-$ is consistent with the formation of cyanide bridge.

Three cyano-bridged Fe^{III}–Mn^{II} dimers, $[Fe(pzcq)(CN)_3][Mn(phen)_2(X)]\cdot MeOH$ (X = Cl or Br) and $[Fe(mpzcq)(CN)_3][Mn(phen)_2(Cl)]\cdot MeOH$ were prepared by assembling molecular precursors, $[Fe(pzcq)(CN)_3]^-$, $[Fe(mpzcq)(CN)_3]^-$ with $Mn(phen)_2X_2$ [39]. $[Fe(pzcq)(CN)_3]^{-1}$ acts as a monodentate ligand through one of its three cyanide groups toward a $[Mn(phen)_2(Cl)]^+$ core (Fig. 2). Each Fe center adopts a distorted octahedral geometry consisting of three C atoms from terminal cyanide ligands and three N atoms from the tridentate ligand. The absolute configurations of the Mn polyhedra surrounded by two bidentate phen ligands are packed in a -Δ-Λ-Δ-Λ- sequence in the crystal lattice. The aromatic rings of the coordinated phen ligands are sources of considerable interdimer π–π contacts, which eventually lead to the formation 2D frameworks. The variable-temperature magnetic susceptibility studies for these three complexes revealed an intradimer antiferromagnetic interaction between the Fe^{III} ($S = 1/2$) and Mn^{II} ($S = 5/2$), giving an $S = 2$ ground state and J_{FeMn} in the range of −2.23 to −3.69 cm^{-1}.

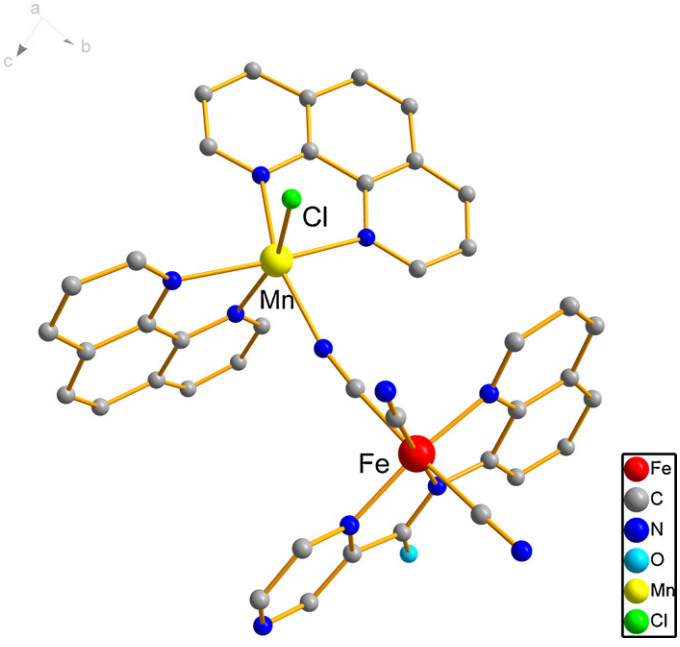

Fig. 2. View of the molecular structure of the dinuclear complex $[Fe(pzcq)(CN)_3][Mn(phen)_2(Cl)]\cdot MeOH$. The solvate methanol molecules have been removed for clarity [39].

In $[(Tp)Fe^{III}(CN)_3Cu^{II}(bipy)_2]ClO_4\cdot CH_3OH$ [40], $[TpFe(CN)_3]^-$ acts as a monodentate ligand toward a central $[Cu(bipy)_2]^{2+}$ core through one of its three cyanide groups, the other two cyanides remaining terminal. Magnetic studies show ferromagnetic coupling between the Cu(II) and Fe(III) ions, giving an $S = 1$ ground state and intradimeric exchange constants $J_{FeCu} = 5.52\ cm^{-1}$. A much strong ferromagnetic interaction between the Fe^{III} and Cu^{II} ions was found in the similar dinuclear complex *fac*-$\{[Fe^{III}(pzTp)(CN)_2(\mu\text{-}CN)]Cu^{II}(TPyA)\}\cdot Et_2O\cdot ClO_4$ ($J_{FeCu} = 11.55\ cm^{-1}$) [41]. This difference is attributed to the presence of short Cu–N bond and more linear Cu–N≡C angle.

The reaction of *mer*-$(PPh_4)[Fe(qcq)(CN)_3]$ and $[Mn^{III}(3\text{-}MeOsalen)(H_2O)]ClO_4$ in a mixture of methanol and water produces $[Fe(qcq)(CN)_3]$ $[Mn(3\text{-}MeOsalen)(H_2O)]\cdot 2H_2O$ [36]. The dimeric unit is constructed from the anionic precursor *mer*-$[Fe(qcq)(CN)_3]^-$ and the cationic $[Mn(3\text{-}MeOsalen)]^+$ part bridged by the cyanide ligand. The structural propagation is blocked by the coordination of one water molecule to one of the binding sites of the Mn Schiff base. A Jahn–Teller apical elongation is evident for the Mn^{III} site. In the extended structure, dimeric moieties are formed by hydrogen bonds among coordinated water molecules and the donor atoms from the qcq ligands, as well as π–π interactions between aromatic rings of qcq ligands. Magnetic susceptibility measurements confirm that the Fe(III)–Mn(III) exchange magnetic coupling is antiferromagnetic ($J_{FeMn} = -4.65\ cm^{-1}$), with a interdimer interaction ($zJ = -0.95\ cm^{-1}$) and a minimal zero-field splitting parameter (D) value of less than 0.01 cm^{-1}. The presence of antiferromagnetic interactions between Mn^{III} and Fe^{III} ions via the CN bridges is consistent with the Fe–Mn systems made of *mer*-Fe tricyanides, $[Fe(mpzcq)(CN)][Mn(salen)(H_2O)]\cdot H_2O$ [34]. In order to obtain the exchange coupling constant, a dimer model based on the spin Hamiltonian $H = -2JS_1S_2$ was used. The molecular-field approximation was taken into consideration to account for the intermolecular magnetic interactions. The magnetic parameters are $g = 2.08$, $J_{FeMn} = -8.6\ cm^{-1}$, and $zJ = -0.62\ cm^{-1}$. The inclusion of the zero-field-splitting term (D) in the fitting process did not improve the result. However, Fe^{III}–Mn^{III} ferromagnetic interactions ($J_{FeMn} = 2.5\text{–}3.74\ cm^{-1}$) have often been reported in some similar dinuclear complex $[Mn(D,L\text{-}Lb)(DMF)(Tp)Fe(CN)_3](H_2O)_6$, $[(Tp)Fe(CN)_3][Mn(1\text{-}napen)(H_2O)]\cdot MeCN\cdot 4H_2O$, $[(Tp)Fe(CN)_3][Mn(5\text{-}Clsalen)(H_2O)]$,

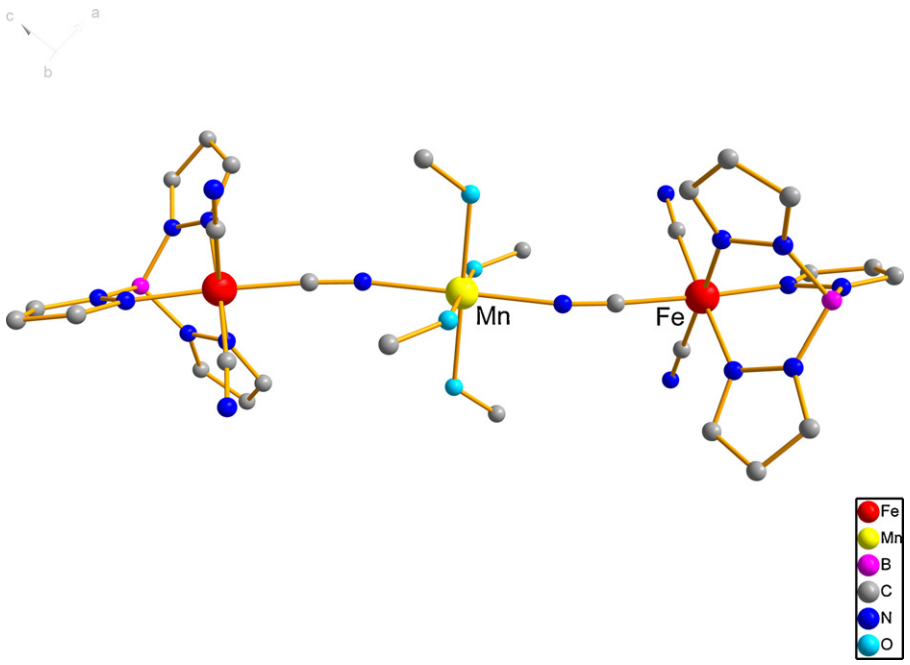

Fig. 3. View of the molecular structure of the trinuclear complex $[(Tp)_2Fe^{III}{}_2(CN)_6Mn(CH_3OH)_4]\cdot 2CH_3OH$. The solvate methanol molecules have been removed for clarity [44,45].

and $[(Tp)Fe(CN)_3]$ [Mn(2-acnapen)(MeOH)]·MeOH, which are built from the *fac*-$[TpFe(CN)_3]^-$ [42,43]. Density Functional Theory (DFT) calculations and comparison of structural parameters show that the ferromagnetic or antiferromagnetic interactions between Mn^{III} and Fe^{III} centers are mainly associated with the bending of the Mn–N≡C angle in the bridging pathway [43].

3.2. Trinuclear cyano-bridged complexes

The first complete characterization of a cyanide bridged trinuclear complex based on the anionic tricyanometalate precursor, $[LFe(CN)_3]^-$, $[(Tp)_2Fe^{III}{}_2(CN)_6Mn(CH_3OH)_4]\cdot 2CH_3OH$ was simultaneously reported by us [44] and by Kim [45]. The crystallographic analysis revealed that each $[TpFe(CN)_3]^-$ unit acts as a monodentate ligand through one of its three cyanide groups toward a central $[Mn(CH_3OH)_4]^{2+}$ core (Fig. 3). The manganese atom is six-coordinated in a squashed octahedral geometry. Four oxygen atoms from the methanol molecules form the equatorial plane. Two cyanide nitrogen atoms occupy the axial positions. The axial Mn–O distances (2.198(2) and 2.1906(19) Å) are slightly shorter than the Mn–N distances (2.174(2) Å). The bond angle of Mn–N≡C (167.2(2)°) departs significantly from 180°. Noncoordinated CH_3OH molecules are inserted into crystal spacing. The magnetic susceptibility data for the complex $[(Tp)_2Fe^{III}{}_2(CN)_6Mn(CH_3OH)_4]\cdot 2CH_3OH$ revealed a weak antiferromagnetic interaction between Fe(III) and Mn(II). This result is in agreement with those in the dinuclear Fe(III)–Mn(II) complex [39] and similar trinuclear complexes $[(Tp)_2Fe^{III}{}_2(CN)_6Mn(C_2H_5OH)_4]\cdot 2C_2H_5OH$ [46], $[(Tp)_2Fe^{III}{}_2(CN)_6Mn(phen)_2]\cdot 5H_2O$ [47], $[(bpca)_2Fe^{III}{}_2(CN)_6Mn(CH_3OH)_2(H_2O)_2]\cdot 2H_2O$ [48], $[(pcq)_2Fe^{III}{}_2(CN)_6Mn(CH_3OH)_2(H_2O)_2]\cdot 2H_2O$, $[(pcq)_2Fe^{III}{}_2(CN)_6Mn(bipy)_2]\cdot CH_3OH\cdot 2H_2O$, and $[(pcq)_2Fe^{III}{}_2(CN)_6Mn(phen)_2]\cdot CH_3OH\cdot 2H_2O$ [49].

Two types of trinuclear Fe(III)–Ni(II)–Fe(III) clusters, namely (i) $[(Tp)_2Fe^{III}{}_2(CN)_6Ni(cyclam)]\cdot 2H_2O$ (cyclam = 1,4,8,11-tetraazacyclotetradecane) [44], $[(Tp)_2Fe^{III}{}_2(CN)_6Ni(en)_2]\cdot 2H_2O$ (en = ethylenediamine) [46] and $[(pzTp)_2Fe^{III}{}_2(CN)_6Ni(L)]\cdot(1/2)CH_3OH$ (L = 1,5,8,12-tetraazadodecane) [28]; (ii) $[(pzTp)_2Fe^{III}{}_2(CN)_6Ni(bipy)_2]\cdot 2H_2O$ [28], have been obtained by the reaction of $[LFe(CN)_3]^-$ and $[Ni(L)]^{2+}$. In the former cases, two $[LFe(CN)_3]^-$ (L = Tp and pzTp) units are linked to one $[Ni(L)]^{2+}$ core (L = cyclam, bipy and 1,5,8,12-tetraazadodecane) to form a nearly linear cluster with the Fe(III)–Ni(II)–Fe(III) angle being in the range of 176.77–180°. The nickel atom is in an elongated octahedral environment. Four nitrogen atoms from the L ligand form the equatorial plane. Two cyanide nitrogen atoms occupy the axial positions in a *trans* geometry. The intramolecular Fe···Ni and Fe···Fe distances are in the range of 4.900(2)–5.132(2) Å and 9.806(2)–10.265(5) Å, respectively. The magnetic susceptibility data indicate the ferromagnetic interaction between the Fe(III) and Ni(II) ions dominates the magnetic properties in these systems, which is in agreement with the field dependence of magnetization, giving an $S = 2$ ground state. AC susceptibility measurements are frequency-independent, suggesting that they are not SMMs in the temperature range measured.

In the later complex, $[(pzTp)_2Fe^{III}{}_2(CN)_6Ni^{II}(bipy)_2]\cdot 2H_2O$ [28], the molecular structure consists of a central $[Ni(bipy)_2]^{2+}$ unit located on a crystallographic mirror plane which is linked to two $[(pzTp)Fe(CN)_3]^-$ anions via *cis*-cyano rather than *trans*-cyano linkages (Fig. 4). The Ni–N≡C bond angle (169.8(4)°) is more linear than the above complexes. Due to the *cis* geometry of the bridging cyanide groups, the intramolecular Fe···Ni and Fe···Fe distances are in the range of 5.080(1) Å and 7.747(1) Å, respectively. The χT vs T data indicate that the Fe and Ni centers are ferromagnetically coupled (Fig. 5a). The χT product gradually increases from 2.34 $cm^{-1}\,K\,mol^{-1}$ (300 K), reaching a maximum value of 4.01 $cm^{-1}\,K\,mol^{-1}$ at 4 K. Below 4 K, χT decreases. Fitting of the magnetic data gives $J = 4.86\ cm^{-1}$ and $g = 2.31$ (Fig. 5a). The magnitude of the magnetic exchange through the cyanide bridges is comparable to those reported for related complexes. The magnetization is nearly saturated, reaching $4\mu_B$ at 7 T. AC susceptibility measurements in a nonzero dc field indicate it is a SMM. The relaxation time follows an Arrhenius law with $\tau_0 = 2 \times 10^{-8}$ s and an

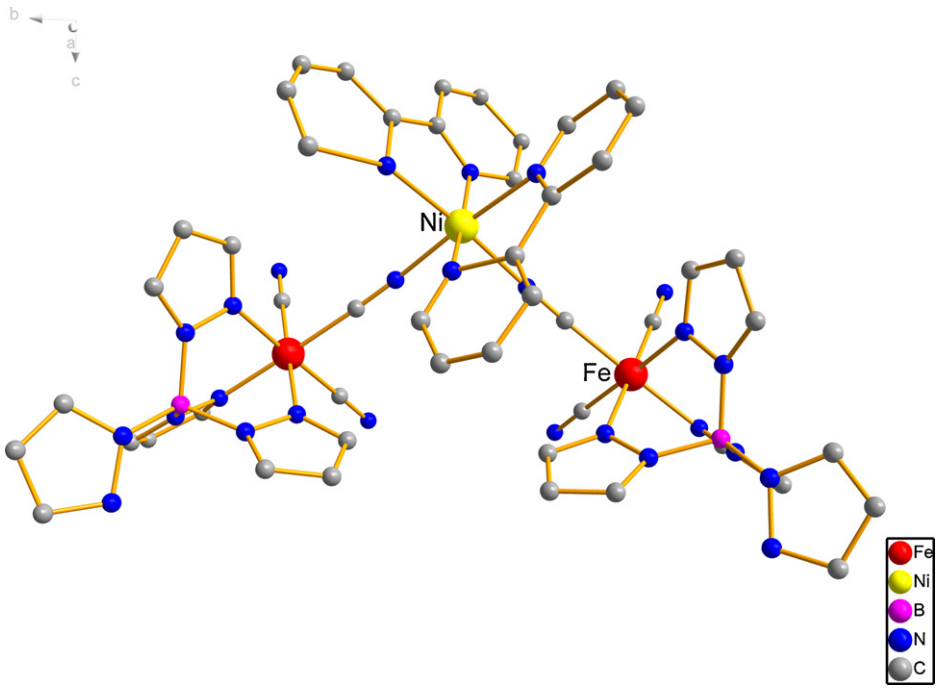

Fig. 4. View of the molecular structure of the trinuclear complex $[(pzTp)_2Fe^{III}{}_2(CN)_6Ni^{II}(bipy)_2]\cdot 2H_2O$. The solvate water molecules have been removed for clarity [28].

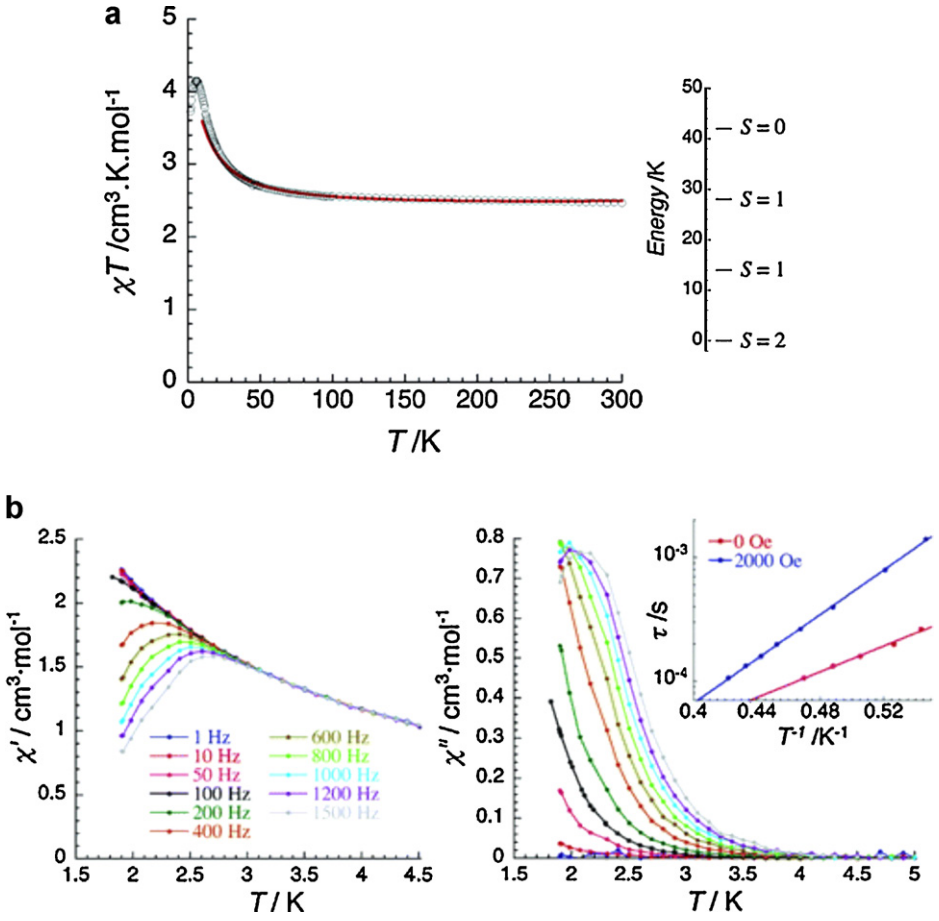

Fig. 5. (a) Temperature dependence of χT at 1000 Oe (left) and energy level diagram (right) for $[(pzTp)_2Fe^{III}{}_2(CN)_6Ni^{II}(bipy)_2]\cdot 2H_2O$. Red line: least-squares fitting of the data. (b) Temperature dependence of the real χ' and imaginary components χ'' of the ac susceptibility (H_{dc} = 0 Oe and H_{ac} = 3 Oe) between 1 and 1500 Hz. Inset τ vs T^{-1} at H_{dc} = 0 and 2000 Oe. The solid lines represent an Arrhenius fit of the data.
Reprinted with permission from Ref. [28]. Copyright 2006 American Chemical Society.

energy gap of 14.4 cm^{-1} is found (Fig. 5b). The energy gap allows an estimation of the uniaxial anisotropy $\Delta/k_B \approx -3.6\,cm^{-1}$.

Recently, two homochiral trinuclear clusters, $\{(MeTp)_2Fe_2(CN)_6Ni[(1R,2R)\text{-chxn}]_2\}$ and $\{(MeTp)_2Fe_2(CN)_6Ni[(1S,2S)\text{-chxn}]_2\}$ (chxn = 1,2-diaminocyclohexane), were synthesized and structurally characterized [50]. Ferroelectric and magnetic measurements reveal that they are rare examples of metal-organic compounds bearing ferroelectricity and intramolecular ferromagnetic interactions.

A series of isostructural linear trinuclear complexes based on $[(Tp)Fe(CN)_3]^-$, $[(Tp)_2Fe^{III}{}_2(CN)_6M^{II}(DMSO)_4]$, ($M^{II}$ = Cu, Ni, Co, Mn; DMSO = dimethylsulfoxide) have been reported by Lu et al. [51]. These complexes are obtained by the reaction of $K[(Tp)Fe(CN)_3]$ and the corresponding $M(NO_3)_2$ (M = Cu, Ni, and Co) or $Mn(Ac)_2$ in water. First, powder sample $[M(H_2O)_4][(Tp)Fe(CN)_3]_2$ was collected, then single crystals were obtained by slow evaporation of THF into a DMSO sample solution. These complexes are isostructural, in which each metal ion is coordinated by two $[(Tp)Fe(CN)_3]^-$ moieties through cyano-bridges in *trans* positions, resulting in a linear trinuclear structure. The temperature dependence of the magnetic data for the complexes (M = Ni, Cu) are consistent with ferromagnetic interactions (J_{FeNi} = 2.68 cm^{-1} and J_{FeCu} = 6.82 cm^{-1}). Based on the magnetic data of the complex $[(Tp)_2Fe^{III}{}_2(CN)_6Co^{II}(DMSO)_4]$, it was found that the bridging cyanide ligands mediate antiferromagnetic interaction between the Co(II) and Fe(III) ions [51]. In the case of M = Mn, contrary to the above similar Fe(III)–Mn(II)–Fe(III) trinuclear complexes, a weak ferromagnetic Fe(III)–Mn(II) interaction (J_{FeMn} = 0.708 cm^{-1}) was found in $[(Tp)_2Fe^{III}{}_2(CN)_6Mn^{II}(DMSO)_4]$. This is attributed to the relationship between the magnetic orbitals of Fe(III), Mn(II) ions and the Mn–N≡C bond angles. The degree of the overlap of the magnetic orbitals of Fe(III) and Mn(II) is proportional to the Mn–N≡C bond angles. The larger magnetic orbitals overlap will lead to stronger Fe(III)–CN–Mn(II) magnetic interactions. Interestingly, the Fe(III)–CN–Mn(II) magnetic coupling inversion takes place along with the decrease of the Mn–N≡C bond angle. The bond angle of Mn–N≡C (154.8(3)°) departs significantly from 180° [51].

Recently, a new cyano-bridged Fe(III)–Fe(II) trinuclear complex, $[Fe_2{}^{III}Fe^{II}(CN)_6(tp^*)_2(tpa)]\cdot 4MeCN\cdot t\text{-}BuMeO$ (tpa = tris(2-pyridylmethyl)amine), was reported [52]. It has a right angled trinuclear core composed of two $[Fe(CN)_3(tp^*)]^-$ and one $[Fe(tpa)]^{2+}$ units (Fig. 6). Coordination bond lengths of Fe–C(cyano) and Fe–N(tpa) are in the range of 1.914(5)–1.933(4) Å and 1.933(4)–1.987(4) Å, respectively, which are characteristic of LS Fe(III) and Fe(II) ions. Magnetic susceptibility measurements were carried out in the temperature range of 5–365 K. The χT values below 250 K are almost constant (1.34 emu mol^{-1} K at 250 K), which corresponds to the theoretical value (1.36 emu mol^{-1} K with g = 2.7) for the uncorrelated two LS Fe(III) ions. As the temperature was increased, the gradual increase of χT values was observed and the χT value reached a maximum value of 2.86 emu mol^{-1} K at 340 K, which corresponds to ca. 50% of the Fe(II) ion being in the high-spin (HS) state, suggesting thermally induced spin crossover.

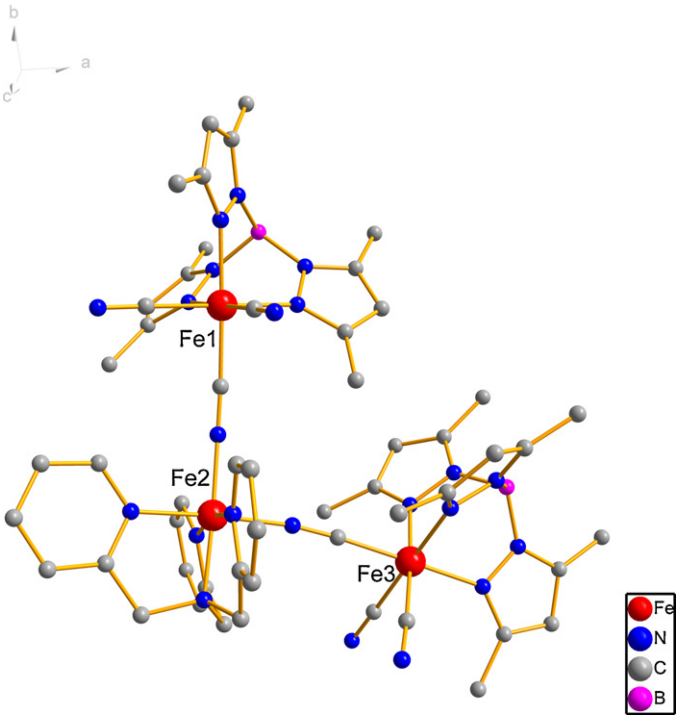

Fig. 6. View of the molecular structure of the trinuclear complex $[Fe_2{}^{III}Fe^{II}(CN)_6(tp^*)_2(tpa)]\cdot 4MeCN\cdot t\text{-}BuMeO$. The solvate molecules have been removed for clarity [52].

3.3. Tetranuclear cyano-bridged complexes

Tetranuclear assembly based on the anionic tricyanometalate precursor, *fac*-$[TpFe(CN)_3]_3[Fe(H_2O)_3]\cdot 6H_2O$, was first reported by Julve et al. in 2002 [26]. The reaction of $Fe(NO_3)_3\cdot 9H_2O$ and $K[(Tp)Fe(CN)_3]$ in aqueous solution resulted in the immediate formation of the product. Good crystals were obtained by slow evaporation of the reaction solution. X-ray crystallography has revealed that it is made up of neutral *fac*-$[(Tp)Fe(CN)_3]_3[Fe(H_2O)_3]$ tetranuclear units and crystallization water molecules. The coordinated and uncoordinated water molecules are linked through an extensive network of hydrogen bonds. $[(Tp)Fe(CN)_3]^-$ acts as a monodentate ligand through one of its three cyanide groups toward a *fac*-triaqua Fe(III) entity affording an original tetranuclear compound where three LS Fe(III) motifs are bound to a central six-coordinated HS Fe(III). Significant ferromagnetic coupling was found between the central spin sextuplet and peripheral spin doublets to give a low-lying S = 4 spin state. The ferromagnetic interaction nature and the nonet ground spin state is indicated also by the magnetization curve at 1.9 K which exhibits a saturation value of ca. 8μ_B at the maximum magnetic field. AC susceptibility measurements, carried out in the temperature range 2–10 K do not show the frequency dependence expected for a single-molecule magnet.

Self-assembly of the anionic building block *fac*-$[LFe(CN)_3]^-$ (L = Tp or Tp*) with various metal ions and blocking ligands have resulted in the formation of square-like tetranuclear clusters. The first square-like tetranuclear complex, $[Mn^{II}{}_2Fe^{III}{}_2Tp_2(CN)_6(bipy)_2](ClO_4)_2\cdot 4MeCN$, was obtained from the reaction of the above trinuclear $[(Tp)_2Fe^{III}{}_2(CN)_6Mn(CH_3OH)_4]\cdot 2CH_3OH$ and $[Mn(bipy)_2(H_2O)_2](ClO_4)_2$ in methanol [45]. The crystal structure consists of a discrete tetranuclear mixed metal complex, two perchlorate anions and four acetonitrile solvent molecules. The overall structure of the cationic complex has been described as a tetranuclear square composed of LS Fe(III) Ions and HS Mn(II) ions (Fig. 7). The $[Fe(Tp)(CN)_3]^-$ coordinates to two adjacent Mn ions with its two linear cyanide bridges. The intramolecular Fe···Mn distances are 5.174(1) and 5.220(1) Å. Magnetic susceptibility shows a weak antiferromagnetic interaction between the Fe(III) and Mn(II) (J_{FeMn} = −2.29(3) cm^{-1}).

After the report on the above square-like tetranuclear complex, interest in heterodimetallic tetranuclear complexes with various metal ions has been long-standing in a few groups and some tetranuclear complexes have

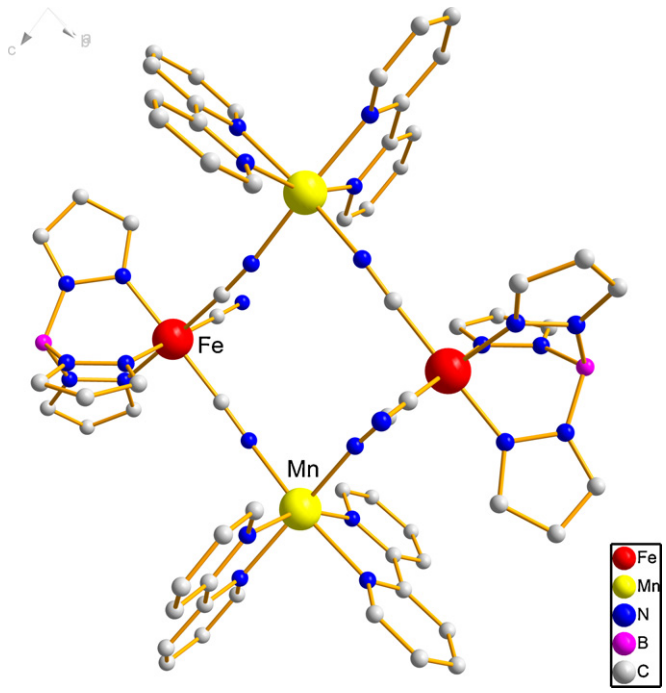

Fig. 7. View of the molecular structure of the tetranuclear complex $[Mn^{II}_2Fe^{III}_2Tp_2(CN)_6(bipy)_2](ClO_4)_2{\cdot}4MeCN$. The anions and solvate molecules have been removed for clarity [45].

been published: (i) $\{[Tp^*Fe^{III}(CN)_3M^{II}(DMF)_4]_2[OTf]_2\}{\cdot}2DMF$ (M^{II} = Mn, Co, Ni; OTf = trifluoromethanesulfonic acid) [53]; (ii) $[TpFe(CN)_3Cu(Tp)]_2{\cdot}2H_2O$, $[TpFe(CN)_3Cu(bpca)]_2{\cdot}4H_2O$, $[TpFe(CN)_3Ni(tren)]_2(ClO_4)_2{\cdot}2H_2O$ (tren = tris(2-aminoethyl)amine), $[TpFe(CN)_3Ni(bipy)_2]_2[TpFe(CN)_3]_2{\cdot}6H_2O$ [54]; (iii) $\{[Tp^*Fe(CN)_3Ni(bipy)_2]_2[OTf]_2\}{\cdot}2H_2O$ [55] $[(pzTp)_2Fe_2Ni_2(dpa)_2(CN)_6](ClO_4)_2{\cdot}2CH_3OH{\cdot}6H_2O$ (dpa = 2,2′-dipyridyl amine) [56]; (iv) $[(phTp)Fe(CN)_3Cu(bipy)(H_2O)(ClO_4)]_2{\cdot}2H_2O$, $[(phTp)Fe(CN)_3Ni(tren)]_2(ClO_4)_2$, $[(MeTp)Fe(CN)_3Ni(tren)]_2(ClO_4)_2{\cdot}2H_2O$, $[(iBuTp)Fe(CN)_3Ni(tren)]_2(ClO_4)_2{\cdot}2H_2O{\cdot}2CH_3OH$ [29].

X-ray crystallographic studies for these compounds have revealed that they possess similar square-like structures. In the square unit, Fe(III) and M(II) ions are located at alternating corners of the rectangle and each $[(Tp)Fe(CN)_3]^-$ unit uses its two cyanides to connect the metal ions, leaving the third terminal cyanide group free.

In the Fe_2Cu_2 clusters, $[TpFe(CN)_3Cu(Tp)]_2{\cdot}2H_2O$ and $[TpFe(CN)_3Cu(bpca)]_2{\cdot}4H_2O$ [54], Cu(II) ions have a distorted square pyramidal coordination sphere, which is completed by three N atoms from the auxiliary ligands and two cyanide nitrogen atoms, however, a elongated distorted octahedral geometry for Cu(II) ions is found in $[(phTp)Fe(CN)_3Cu(bipy)(H_2O)(ClO_4)]_2{\cdot}2H_2O$ [29]. Similar to the dinuclear and trinuclear complexes, the Fe_2Cu_2 square clusters show a ferromagnetic interaction between the Fe(III) and Cu(II) through the cyanide bridges (J_{FeCu} = 1.38–11.91 cm^{-1}). The magnetization measurements confirm the nature of ferromagnetic interaction and the ground state of $S = 2$. AC susceptibility studies carried out in the 1.8–10 K range showed no evidence for magnetic ordering or slow paramagnetic relaxation.

Magnetic measurements indicate that the bridging cyanide ligands mediate ferromagnetic interaction between the Ni(II) and Fe(III) ions (with J_{FeNi} in the range of 2.84–7.36 cm^{-1}) in the Fe_2Ni_2 squares. All the Fe_2Ni_2 squares exhibits an $S = 3$ ground state, slow relaxation of the magnetization and SMM behavior, except unusual spin-glass-like dynamic relaxations are observed for complex $[TpFe(CN)_3Ni(bipy)_2]_2[TpFe(CN)_3]_2{\cdot}6H_2O$. The single-ion anisotropy contributions of the Ni(II) centers are of minor importance in tuning the magnetic relaxation behavior of these tetranuclear complexes and the height of the magnetization reversal barrier is largely dependent on the single-ion anisotropy contributions of the LS Fe(III) centers. Antiferromagnetic interaction between the Co(II) and Fe(III) ions (with $J_{FeCo} = -10\ cm^{-1}$) was found in the Fe_2Co_2 cluster, $\{[Tp^*Fe^{III}(CN)_3Co^{II}(DMF)_4]_2[OTf]_2\}{\cdot}2DMF$ [53].

Four tetranuclear heterometallic compounds, $[LFe(CN)_3]_2[Ru_2(DMBA)_4]$ (L = Tp, MeTp, *i*BuTp, phTp; DMBA = N,N-dimethylbenzamidinate) were prepared from the combination of $Ru_2(DMBA)_4(NO_3)_2$ and an appropriate $[LFe(CN)_3]^-$ [57]. Molecular structures of these compounds feature a linear Fe–C≡N–Ru–Ru–N≡C–Fe array. The $[LFe(CN)_3]^-$ complex occupies each of the axial sites of [Ru(DMBA)] via the N coordination to the Ru center by a cyanide ligand, which confirm the formation of 'a complex of complexes'. The magnetic study revealed that the temperature dependence of χT is mostly attributed to the zero-field splitting of the Ru_2 center (D = 168.29–212.27 cm^{-1}), indicating the absence of strong exchange coupling among three metallic centers. The electronic independence was confirmed by the vis–NIR spectroscopic studies.

Three cyano-linked Fe(III)–Mn(III) bimetallic clusters, $[(Tp)Fe(CN)_3]_2[Mn(acphen)]_2$ (acphen = *N*,*N*′-ethylenebis(2-hydroxyacetophenylideneiminato) dianion), $[(Tp)Fe(CN)_3]_2[Mn(5\text{-}Bracphen)]_2$ (5-Bracphen = *N*,*N*′-ethylenebis(5-bromo-2-hydroxyacetophenylideneiminato) dianion), and $[(Tp)Fe(CN)_3]_2[Mn(salen)]_2{\cdot}6H_2O$ were prepared by self-assembling a facial $[(Tp)Fe(CN)_3]^-$ precursor and the respective Mn(III) Schiff bases [58]. X-ray crystal structure analyses revealed that each complex is composed of a central Mn(III) dimer doubly linked by phenoxides of the tetradentate N_2O_2 Schiff bases and the terminal $[(Tp)Fe(CN)_3]^-$ groups connecting to the center through cyanides (Fig. 8). Using the spin Hamiltonian $H = -2J_1(S_{Fe1}S_{Mn1} + S_{Mn1a}{\cdot}S_{Fe1a}) - 2J_2(S_{Mn1}{\cdot}S_{Mn1a})$, where J_1 stands for the exchange coupling constant between Fe(III) ($S_{Fe} = 1/2$) and Mn(III) ($S_{Mn} = 2$) through cyanides and J_2 between Mn(III) ions via phenoxides, the best fits corresponded to $J_1 = 2.61\ cm^{-1}$ and $J_2 = 0.85\ cm^{-1}$ for $[(Tp)Fe(CN)_3]_2[Mn(acphen)]_2$, $J_1 = 2.50\ cm^{-1}$ and $J_2 = 1.30\ cm^{-1}$ for $[(Tp)Fe(CN)_3]_2[Mn(5\text{-}Bracphen)]_2$, and $J_1 = -2.15\ cm^{-1}$ and $J_2 = 0.55\ cm^{-1}$ for $[(Tp)Fe(CN)_3]_2[Mn(salen)]_2{\cdot}6H_2O$. The phenoxide routes transmit ferromagnetic interactions in all cases, while ferromagnetic or antiferromagnetic coupling occurs through the cyanide linkage. Although *fac*-tricyanides mediate ferromagnetic coupling in most of the dinuclear Fe^{III}–Mn^{III} systems [43], the geometric parameters relevant to the magnetic Fe–C≡N–Mn pathways are analogous to each other their magnetic natures are varied, which means that a degree of orbital overlap is quite sensitive to a subtle structural change in the present systems.

3.4. Pentanuclear complexes

The reactions of $[M^{II}(Tpm(Me))(H_2O)_3]^{2+}$ (M = Ni, Co, Fe; Tpm(Me) = tris(3,5-dimethyl-1-pyrazoyl) methane) with $[NBu_4][(Tp)Fe^{III}(CN)_3]$ in MeCN–Et_2O afford three pentanuclear cyano-bridged clusters, $[(Tp)_3(Tpm(Me))_2(Fe^{III}_3M^{II}_2)(CN)_9]ClO_4{\cdot}15H_2O$ (M = Ni, Co) and $[(Tp)_3(TpmMe)_2(Fe^{III}_3Fe^{II}_2)(CN)_9]BF_4{\cdot}15H_2O$ [59].

Clusters $Fe_3^{III}Ni_2^{II}$ and $Fe_3^{III}Fe_2^{II}$ are isostructural and crystallize in the trigonal $P3c1$ space group, with a well-isolated $[(Tp)_3(Tpm(Me))_2Fe_3M_2(CN)_9]^+$ cluster. As shown in Fig. 9, both clusters have the trigonal bipyramid geometry featuring a D_{3h} symmetry core in which two octahedral $[M(Tpm)(Me)]^{2+}$ units situated in the apical positions

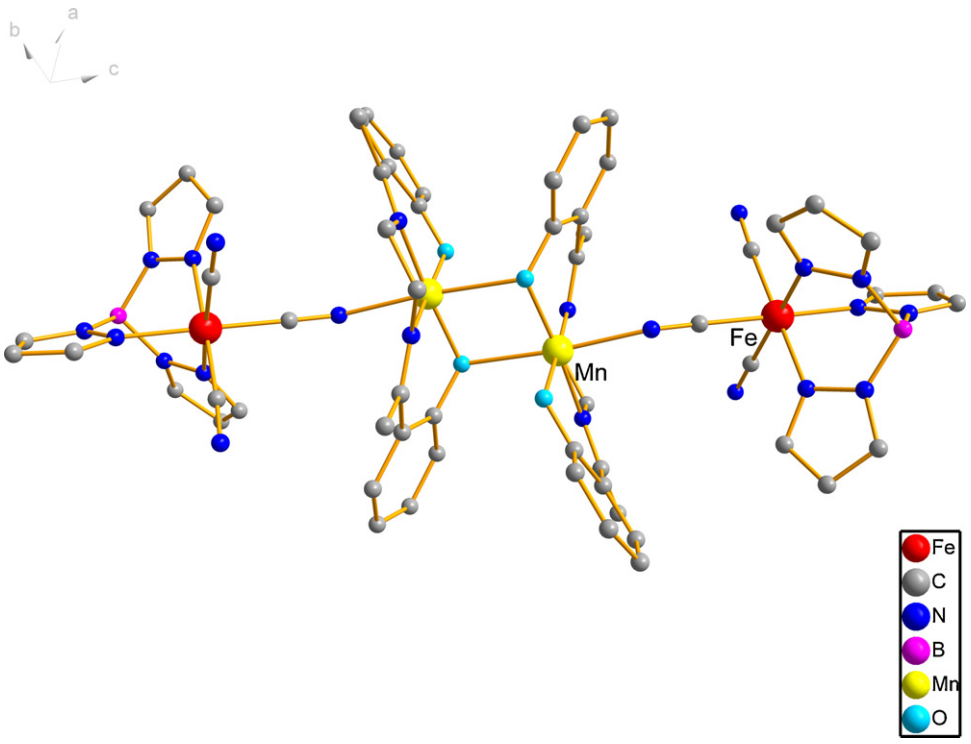

Fig. 8. View of the molecular structure of the tetranuclear complex $[(Tp)Fe(CN)_3]_2[Mn(acphen)]_2$ [58].

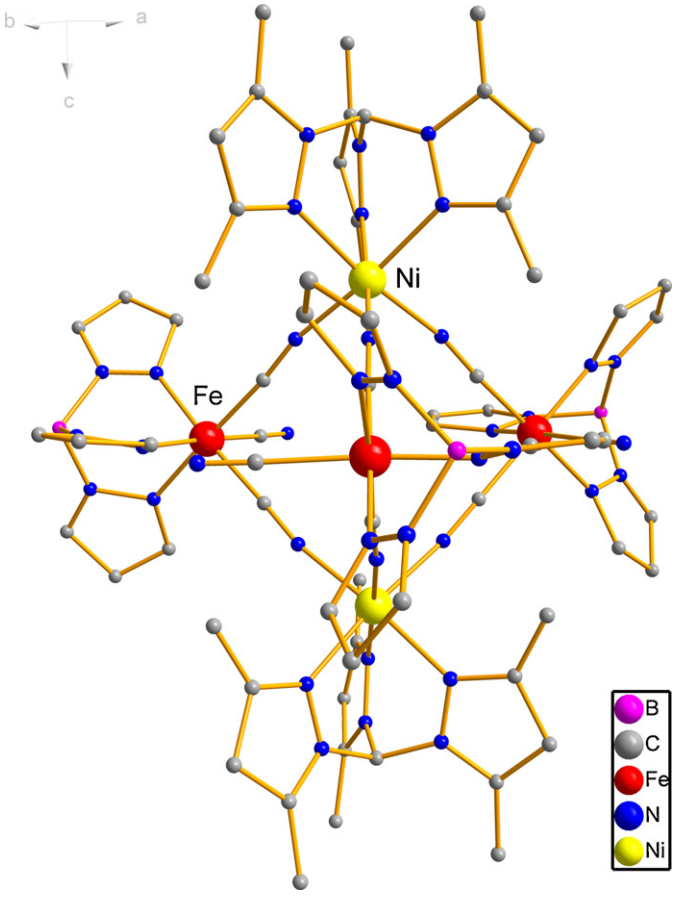

Fig. 9. View of the molecular structure of the pentanuclear complex $[(Tp)_3(Tpm(Me))_2(Fe^{III}_3Ni^{II}_2)(CN)_9]ClO_4{\cdot}15H_2O$. The perchlorate anions and the solvate water molecules have been removed for clarity [59].

are bridged through CN groups to three octahedral $[(Tp)Fe(CN)_3]^-$ units that occupy the equatorial plane. Each Fe ion is linked to M centers through two of its three nearly linear cyanide bridges and is capped by the tridentate Tp ligand.

Magnetic studies for cluster $Fe_3{}^{III}Ni_2{}^{II}$ show ferromagnetic coupling between the Fe^{III} and Ni^{II} ($g = 2.27$, $J = 4.84\,cm^{-1}$) giving an $S = 7/2$ ground state and an appreciable magnetic anisotropy with a negative value ($D = -0.79\,cm^{-1}$). The orthogonality of the magnetic orbital for Ni and Fe ions leads to ferromagnetic interaction and the low-symmetry space group results in the overall negative molecular anisotropy. A ferromagnetic interaction was observed in the cluster $Fe_3{}^{III}Co_2{}^{II}$, between the Fe^{III} and Co^{II}; the magnetization data yielded $D = -1.33\,cm^{-1}$ and $g = 2.81$. However, AC susceptibility studies carried out in the 1.8–10 K range in a 5 Oe oscillating field at frequencies up to 1500 Hz for these complexes showed no evidence for magnetic ordering or slow paramagnetic relaxation. An antiferromagnetic interaction between the LS Fe^{III} and HS Fe^{II} was observed in cluster $Fe_3{}^{III}Fe_2{}^{II}$. Using an approximate isotropic model, the χT value was fitted above 40 K, giving $g = 2.065$ and $J = -0.74(4)\,cm^{-1}$.

The reactions of $(NBu_4)[(Tp^*)Fe(CN)_3]$ ($Tp^* = Tp$, Tp^{4Bo} = tris(indazolyl)hydroborate) with $[Cu(Me_3tacn)(H_2O)_2](ClO_4)_2$ (Me_3tacn = N,N′,N″-trimethyl-1,4,7-triazacyclononane) afford three pentanuclear cyano-bridged clusters, $[(Tp)_2(Me_3tacn)_3Cu_3Fe_2(CN)_6](ClO_4)_4{\cdot}2H_2O$, [60], $[(Tp^{4Bo})_2(Me_3tacn)_3Cu_3Fe_2(CN)_6](ClO_4)_4{\cdot}5H_2O$, and $[(pzTp)_2(Me_3tacn)_3Cu_3Fe_2(CN)_6](ClO_4)_4{\cdot}4H_2O$ [61]. Their molecular structures were determined by single-crystal X-ray diffraction. The crystal structures are very similar and are depicted in Fig. 10. Complexes $[(Tp)_2(Me_3tacn)_3Cu_3Fe_2(CN)_6](ClO_4)_4{\cdot}2H_2O$ and $[(pzTp)_2(Me_3tacn)_3Cu_3Fe_2(CN)_6](ClO_4)_4{\cdot}4H_2O$ crystallize in the monoclinic $P2_1/c$ space group while complex $[(Tp^{4Bo})_2(Me_3tacn)_3Cu_3Fe_2(CN)_6](ClO_4)_4{\cdot}5H_2O$ crystallizes in the tetragonal $P4/mnm$ space group. All clusters have a trigonal bipyramidal geometry, in which three square-pyramidal $[Cu(Me_3tacn)]^{2+}$ units are situated in the equatorial plane that

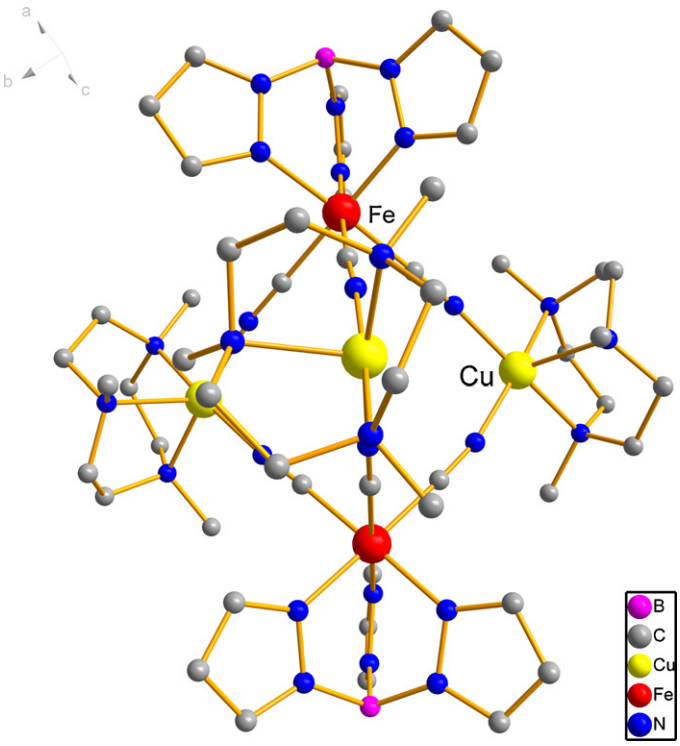

Fig. 10. View of the molecular structure of the pentanuclear complex $[(Tp)_2(Me_3tacn)_3Cu_3Fe_2(CN)_6](ClO_4)_4{\cdot}2H_2O$. The perchlorate anions and the solvate water molecules have been removed for clarity [60].

are bridged through cyanides to two $[(L)Fe(CN)_3]^-$ units occupying the apical positions. Each Fe^{III} ion possesses an octahedral coordination environment. The Cu ions are coordinated to a Me_3tacn ligand as well as two nitrogens atoms of two cyanide bridges, forming a square-pyramidal coordination conformation. The basal positions of the square pyramid are occupied by two cyanide nitrogen atoms and two Me_3tacn nitrogen atoms. Intramolecular ferromagnetic coupling is observed for these complexes, and they have $S = 5/2$ ground states and appreciable magnetic anisotropies with negative D values equal to -5.7, -0.49, and $-2.39\,cm^{-1}$, respectively. However, the structural symmetry distortion of the cluster core has significant impact on the overall magnetic anisotropy. Furthermore, the obvious crystallographic disorder and inter molecular C–H stacking interactions in $[(pzTp)_2(Me_3tacn)_3Cu_3Fe_2(CN)_6](ClO_4)_4{\cdot}4H_2O$ may also account for the significantly decreased axial anisotropy. AC susceptibility measurements in a zero dc field indicate complex $[(Tp)_2(Me_3tacn)_3Cu_3Fe_2(CN)_6](ClO_4)_4{\cdot}2H_2O$ is a SMM. The relaxation time follows an Arrhenius law with $\tau_0 = 4.8 \times 10^{-8}$ s and an effective energy reversal barrier of $16\,cm^{-1}$ is found despite the ground state being $S = 5/2$ (Fig. 11) [60].

Recently, Long and co-workers reported a new pentanuclear cyano-bridged cluster, $[(Tp)_2(cyclen)_3Ni^{II}{}_3Fe^{III}{}_2(CN)_6](BF_4)_4$ (cyclen = 1,4,7,10-tetraazacyclododecane), with a similar trigonal bipyramid geometry [62]. The temperature-dependence of the magnetization under varying applied field reveals significant axial anisotropy, with a ground state of $S = 4$ and axial zero-field splitting ($D = -1.7\,cm^{-1}$). AC magnetic susceptibility measurements reveal a frequency-dependent out-of-phase signal suggestive of SMM behavior.

3.5. Hexanuclear complexes

Attempts to prepare different cyano-bridged assemblies based on the anionic tricyanometalate precursor, $[LFe(CN)_3]^-$, have illus-

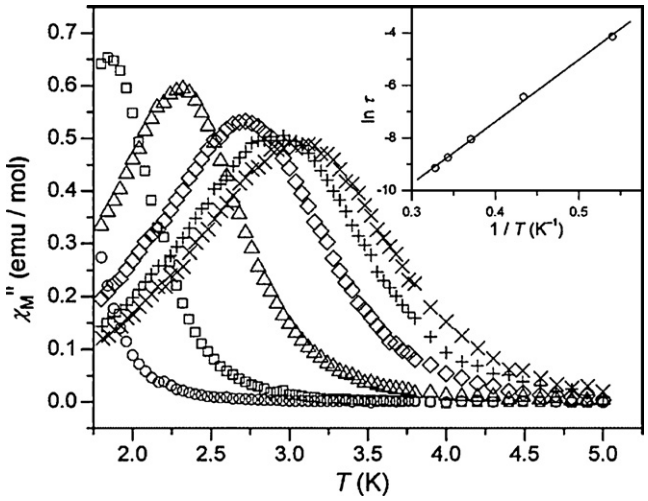

Fig. 11. Out-of-phase of the ac magnetic susceptibility data for $[(Tp)_2(Me_3tacn)_3Cu_3Fe_2(CN)_6](ClO_4)_4{\cdot}2H_2O$, recorded with switching frequencies of 1(○), 10 (□), 100 (△), 499 (◊), 997 (+), 1488 (×) Hz. Inset: Arrhenius law fit of peak maximum as a function of relaxation time.
Reprinted with permission from Ref. [60]. Copyright 2006 American Chemical Society.

trated that the types of complexes to be formed are quite dependent on the starting metal salts and the solvents used. In one case, using mixed solvents have led to the isolation of the hexanuclear complexes: $[\{Fe(Tp)(CN)_3\}_4\{M(MeCN)(H_2O)_2\}_2]{\cdot}10H_2O{\cdot}2MeCN$ [M^{II} = Ni, Co, Mn [63], M^{II} = Fe [64]].

In general, the Fe_4M_2 hexanuclear complexes are obtained by stoichiometric reaction of $[(Tp)Fe(CN)_3]^-$ and $M(ClO_4)_2{\cdot}6H_2O$ or $M(NO_3)_2$ in a mixture of acetonitrile and water. The structure is a neutral Fe_4M_2 hexanuclear cluster, in which two $[(Tp)Fe(CN)_3]^-$ anions act as bidentate ligands to bridge two M(II) ions through cyanides bridges in the *cis* positions to construct a molecular square $[Fe_2M_2(CN)_4]^{6+}$ (Fig. 12). The remaining coordination sites of each six-coordinated M(II) ion are occupied by one monodentate $[(Tp)Fe(CN)_3]$ anion, a MeCN molecule, and two water molecules. The overall $[Fe_4M_2(CN)_6]^{10+}$ unit is approximately coplanar. The intramolecular Fe–M separations are in the range of 5.071–5.206 Å, which are comparable to those in the tetranuclear Fe_2M_2 square. Ten unbound H_2O and two MeCN molecules exist between cyano-bridged Fe_4M_2 clusters. The Fe_4M_2 molecules are linked through hydrogen bonds involving coordinated, uncoordinated water molecules and nitrogen atoms of terminal CN groups. Magnetic studies demonstrate antiferromagnetic intracluster coupling in $Fe^{III}{}_4Mn^{II}{}_2$, $Fe^{III}{}_4Fe^{II}{}_2$ and $Fe^{III}{}_4Co^{II}{}_2$ clusters, which are in accord with unpaired electron orbital symmetry. However, facile loss of solvent from $[\{Fe(Tp)(CN)_3\}_4\{Co(MeCN)(H_2O)_2\}_2]{\cdot}10H_2O{\cdot}2MeCN$, alters the local symmetry resulting in changing the intracluster interaction from antiferro- to ferromagnetic.

The $Fe^{III}{}_4Ni^{II}{}_2$ cluster is a canted antiferromagnet that undergoes a field-induced spin-flop-like transition at 1 T at 2 K. At 4.45 K it undergoes a transition to paramagnetic state of non interacting $S = 4$ magnetic clusters. On further warming, the relatively weak intracluster ferromagnetic coupling fails to compete with thermal agitation, and the material behaves as independent octahedral $S = 1/2$ LS Fe^{III} and $S = 1$ Ni ions [63].

3.6. Octanuclear complexes

Self-assembly of the anionic building block *fac*-$[LFe(CN)_3]^-$ and metal ions in the presence of various blocking ligands have sometimes resulted in the formation of octanuclear box-like clusters: (i) $[(pzTp)Fe^{III}(CN)_3]_4[Ni^{II}L]_4[OTF]_4{\cdot}10DMF{\cdot}Et_2O$ (L = 2,2,2-

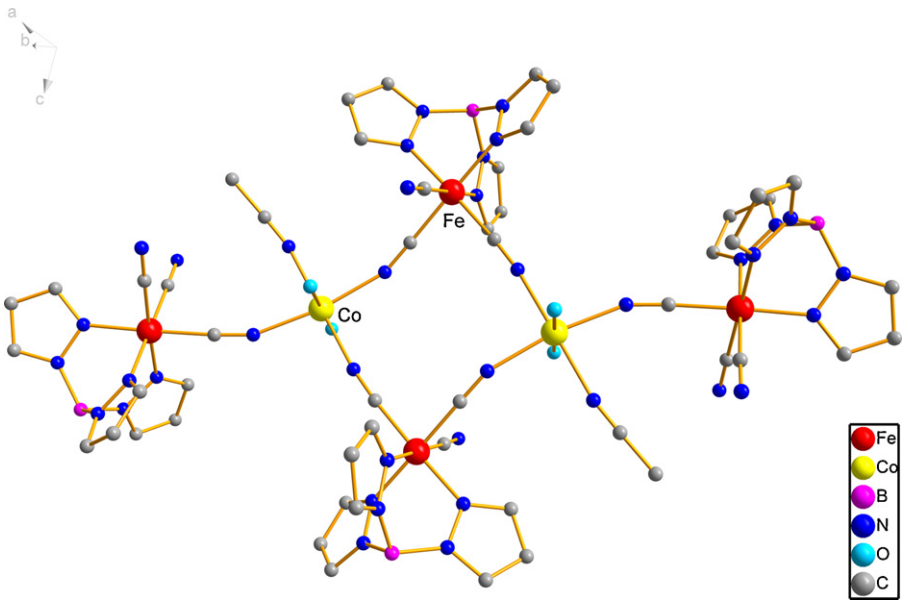

Fig. 12. View of the molecular structure of the hexanuclear complex $[\{Fe(Tp)(CN)_3\}_4\{M(MeCN)(H_2O)_2\}_2]\cdot 10H_2O\cdot 2MeCN$. The solvate molecules have been removed for clarity [63].

tris(pyrazolyl)ethanol) [65], $[(pzTp)Fe^{III}(CN)_3]_4[Ni^{II}L]_4[OTF]_4$ (L = 1-S(acetyl)-tris(pyrazolyl)hexane) [66], $[(pzTp)_4(phen)_4Ni^{II}_4Fe^{III}_4(CH_3OH)_4(CN)_{12}]_4(ClO_4)_4\cdot 4H_2O$ [61]; (ii) $[(pzTp)Fe^{III}(CN)_3]_4[Co^{II}L(CH_3OH)]_4[ClO_4]_4\cdot 13DMF\cdot 4H_2O$ (L = 2,2,2-tris(pyrazolyl)ethanol) [67]; (iii) $[Fe^{II}_4Fe^{III}_4(CN)_{12}(Tp)_8]_4\cdot 12DMF\cdot 2Et_2O\cdot 4H_2O$ [68], $[(BF_4)\cdot\{Fe^{II}(H_2O)\}_4\{(HC(3,5\text{-}Me_2Pz)_3Fe^{II}(CN)_3)\}_4](BF_4)_3$ [69]; (iv) $[(Tp^{*Me})_4Fe^{III}(CN)_3]_4[Ni^{II}(tren)_4]_4(ClO_4)_4\cdot 7H_2O\cdot 4MeCN$ (Tp^{*Me} = tris(3,4,5-trimethylpyrazolyl)borate) [70]. The synthesis of these complexes employs the reaction of the metal(II) salts (M = Fe(II), Ni(II), Co(II)) and $[LFe(CN)_3]^-$ in a 1:1 stoichiometry and in the presence of the corresponding blocking organic ligand (in excess with respect to M(II)).

The first cyano-bridged octanuclear box-like cluster based on *fac*-$[LFe(CN)_3]^-$, $[(pzTp)Fe^{III}(CN)_3]_4[Ni^{II}L]_4[OTF]_4\cdot 10DMF\cdot Et_2O$ (L = 2,2,2-tris(pyrazolyl)ethanol), was reported by Holmes and coworkers [65]. The crystallographic analysis revealed the formation of a cationic box-like cluster crystallizing in the tetragonal $I4_1/acd$ space group. The Fe and Ni centers reside in alternate corners of the slightly distorted molecular box and are linked via cyanides into Fe–(μ-CN)–Ni units; the bridging cyanides are located on the cube edges (Fig. 13). The average edge (FeNi), face (FeFe), and body diagonal (FeNi) distances are ca. 5.120(3), 7.364(4), and 8.858(4) Å, respectively. Ferromagnetic coupling was found between the LS Fe(III) and Ni(II) ions, giving a $g_{iso} = 2.20(5)$ and $J_{FeNi} = 6.6\,cm^{-1}$. Least-squares fitting of the *M* vs *H*/T data affords $D/k = -0.23\,cm^{-1}$, suggesting that the maximum energy barrier is $8.28\,cm^{-1}$ (Fig. 14). AC magnetic susceptibility measurements reveal a very small frequency-dependent out-of-phase signal. However, in the presence of small magnetic field, slow relaxation of the magnetization is clearly seen, suggestive of SMM behavior. Attempts to increase the anisotropy of the Fe_4Ni_4 cluster by using other blocking ligands have resulted in the formation of similar box-like octanuclear complexes $[(pzTp)Fe^{III}(CN)_3]_4[Ni^{II}L]_4[OTF]_4$ (L = 1-S(acetyl)-tris(pyrazolyl)hexane) [66] and $[(pzTp)_4(phen)_4Ni^{II}_4Fe^{III}_4(CH_3OH)_4(CN)_{12}]_4(ClO_4)_4\cdot 4H_2O$ [61]. They all exhibit the slow relaxation of the magnetization.

A similar box-like structure has been reported for $[(pzTp)Fe^{III}(CN)_3]_4[Co^{II}L(CH_3OH)]_4[ClO_4]_4\cdot 13DMF\cdot 4H_2O$ (L = 2,2,2-tris(pyrazolyl)ethanol) [67]. Electron transfer within this octanuclear complex (below 250 K) that converts paramagnetic red crystals into green diamagnetic ones has been confirmed by spectroscopic, magnetic, and crystallographic methods. The color and magnetic changes are associated with the transformation of Fe^{III}_{LS}–CN–Co^{II}_{HS} units into Fe^{II}_{LS}–CN–Co^{III}_{LS} fragments. Moreover, this intramolecular electron transfer can be quantitatively circumvented via rapid thermal quenching and reversed via simple white light irradiation at low temperatures. The thermally or photoinduced paramagnetic metastable phases are identical and exhibit long relaxation times that approach 10 years at 120 K.

The reaction of $(NBu_4)[Fe^{III}(CN)_3(Tp)]$ with $Fe^{II}(OTf)_2\cdot 4H_2O$ and K(Tp) yielded the neutral octanuclear complex $[Fe^{II}_4Fe^{III}_4(CN)_{12}(Tp)_8]_4\cdot 12DMF\cdot 2Et_2O\cdot 4H_2O$ as green cubic

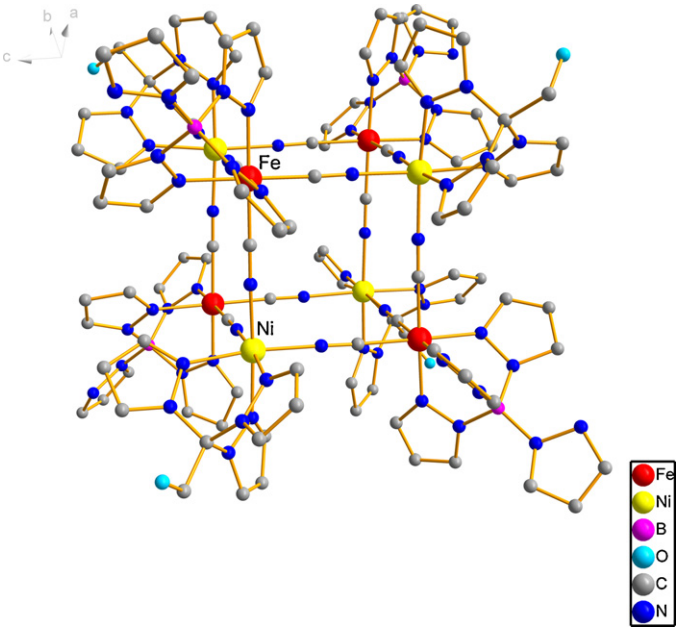

Fig. 13. View of the molecular structure of the octanuclear complex $[(pzTp)Fe^{III}(CN)_3]_4[Ni^{II}L]_4[OTF]_4\cdot 10DMF\cdot Et_2O$ (L = 2,2,2-tris(pyrazolyl)ethanol). The anions and the solvate molecules have been removed for clarity [65].

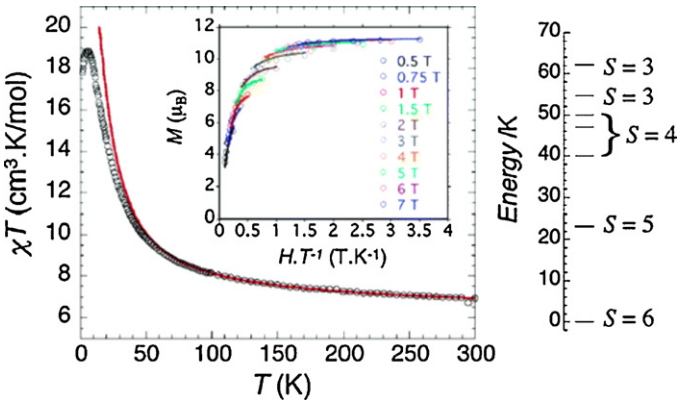

Fig. 14. χT vs T plot for $[(pzTp)Fe^{III}(CN)_3]_4[Ni^{II}L]_4[OTF]_4{\cdot}10DMF{\cdot}Et_2O$ at $H = 0.1T$ (left). Redline: MAGPACK simulation of the data above 30 K. (Inset) Plot of reduced magnetization vs H/T between 2 and 5 K. Solid lines represent least-squares fitting of the data. Diagram of the first seven energy levels (right).
Reprinted with permission from Ref. [65]. Copyright 2006 American Chemical Society.

crystals [68] with a box-like structure similar to the above discussed Fe_4Ni_4 and Fe_4Co_4 clusters. Electron transfers from $[(Tp)Fe^{III}(CN)_3]^-$ to $[(Tp)Fe^{II}]^+$ sites occur during the reaction, leading to Fe^{II}–CN–Fe^{III} oxidation. In the IR spectrum, there are three peaks at 2098, 2079, and 2057 cm^{-1}, which can be assigned to stretches characteristic of M^{II}–CN–M^{III} bridges. The weak antiferromagnetic interactions between HS Fe^{III} ions are operative in the cube. A cyclic voltammogram showed quasi-reversible four-stepped redox waves, which correspond to $[Fe^{III}{}_4Fe^{II}{}_4]/[Fe^{III}{}_5Fe^{II}{}_3]^+$, $[Fe^{III}{}_5Fe^{II}{}_3]^+/[Fe^{III}{}_6Fe^{II}{}_2]^{2+}$, $[Fe^{III}{}_6Fe^{II}{}_2]^{2+}/[Fe^{III}{}_7Fe^{II}{}_1]^{3+}$, $[Fe^{III}{}_7Fe^{II}{}_1]^{3+}/[Fe^{III}{}_8]^{4+}$ processes.

Recently, Hsu and co-workers reported the reaction of diamagnetic $K[(HC(3,5\text{-}Me_2Pz)_3)Fe^{II}(CN)_3]$ and $Fe^{II}(BF_4)_2{\cdot}6H_2O$ leads to the formation of the first cyanometallate cage containing an anion template inside the cage, $[(BF_4)\cap\{Fe^{II}(H_2O)\}_4\{(HC(3,5\text{-}Me_2Pz)_3Fe^{II}(CN)_3)\}_4](BF_4)_3$ [69]. The Fe_8 cubic cage is an air sensitive yellow compound that becomes insoluble green product after exposure to air.

Treatment of $(NEt_4)[(Tp^{*Me})Fe(CN)_3]$ with nickel perchlorate and tren in methanol affords $[(Tp^{*Me})_4Fe^{III}(CN)_3]_4[Ni^{II}(tren)_4]_4(ClO_4)_4{\cdot}7H_2O{\cdot}4MeCN$ as red plates [70] crystallizing as a low symmetrical tetra-cationic octanuclear species in the triclinic P-1 space group. The polynuclear complex consists of two crystallographically independent Fe^{III} and Ni^{II} ions that are linked via cyanide bridges to form a central $\{Fe^{III}{}_2Ni^{II}{}_2\}$ square linked to two adjacent bimetallic $\{Fe^{III}Ni^{II}\}$ units (Fig. 15). Intramolecular ferromagnetic coupling is observed between the Fe^{III} and Ni^{II} ions with $J_{FeNi} = +6.6\ cm^{-1}$ and $g_{avg} = 2.4(1)$, suggesting an $S = 6$ ground state (Fig. 16a). The uniaxial magnetic anisotropy is present. The D and g values are estimated to be $-0.89\ cm^{-1}$ and 2.60(5), respectively, differ markedly from those seen for the cubic $Fe^{III}{}_4Ni^{II}{}_4$ clusters ($-0.23\ cm^{-1}$ and 2.2) [61,65,66]. The AC susceptibility above 1.8 K is frequency dependent on both in-phase and out-of-phase components (Fig. 16b). The energy barrier ($\Delta/k_B \approx 23\ cm^{-1}$) for magnetization reversal is the highest seen for any first-row cyano-based complex. Compared to the above cubic $Fe^{III}{}_4Ni^{II}{}_4$ boxes, the anisotropy axes alignment and the overall lower symmetry have big impact on its SMM properties.

3.7. Fourteen-nuclear cyano-bridged complexes

We reported the first fourteen nuclear cyano-bridged complex based on *fac*-$[LFe(CN)_3]^-$, $[(Tp)_8(H_2O)_6Cu_6Fe_8(CN)_{24}](ClO_4)_4{\cdot}12H_2O{\cdot}2Et_2O$, in 2004 [71]. The slow diffusion of ether vapor into an acetonitrile solution of $(NBu_4)[TpFe(CN)_3]$ and $Cu(ClO_4){\cdot}6H_2O$ results in the formation of the cluster, crystallizing in the space group *Immm*, with well-isolated $[(Tp)_8(H_2O)_6Cu_6Fe_8(CN)_{24}]^{4+}$ molecules residing on special positions of *mmm* site symmetry. As shown in Fig. 17, the clusters adopt a face-centered cubic geometry, in which eight Tp^--capped Fe^{III} ions are arranged in a cube and linked through cyanide to six Cu^{II} ions located just above the center of each cube face. Each octahedral $[(Tp)Fe(CN)_3]^-$ unit uses three cyanide groups to connect with three Cu^{II} ions, which are further ligated by water to give

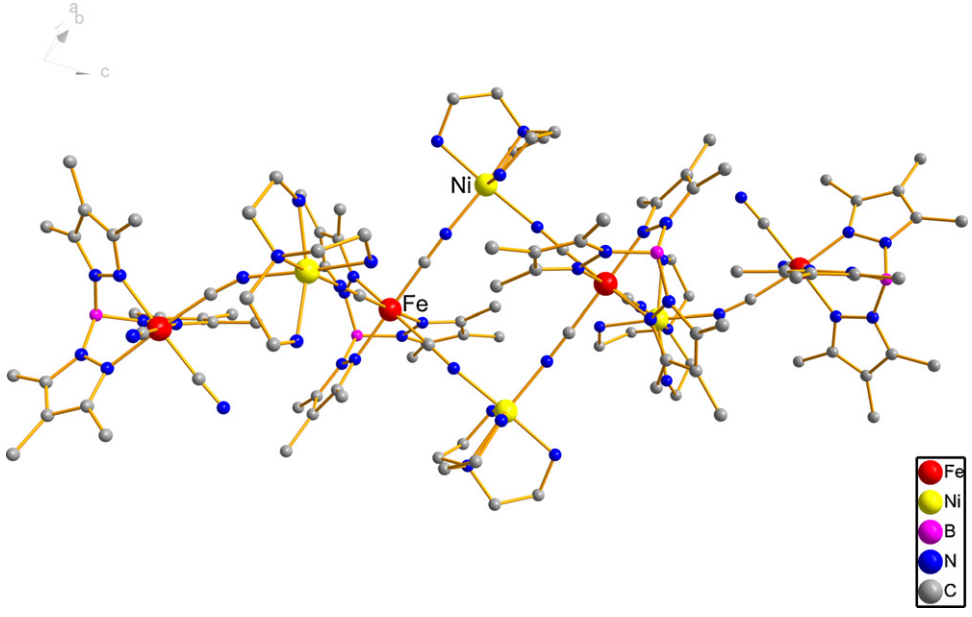

Fig. 15. View of the molecular structure of the octanuclear complex $[(Tp^{*Me})_4Fe^{III}(CN)_3]_4[Ni^{II}(tren)_4]_4(ClO_4)_4{\cdot}7H_2O{\cdot}4MeCN$. The anions and the solvate molecules have been removed for clarity [70].

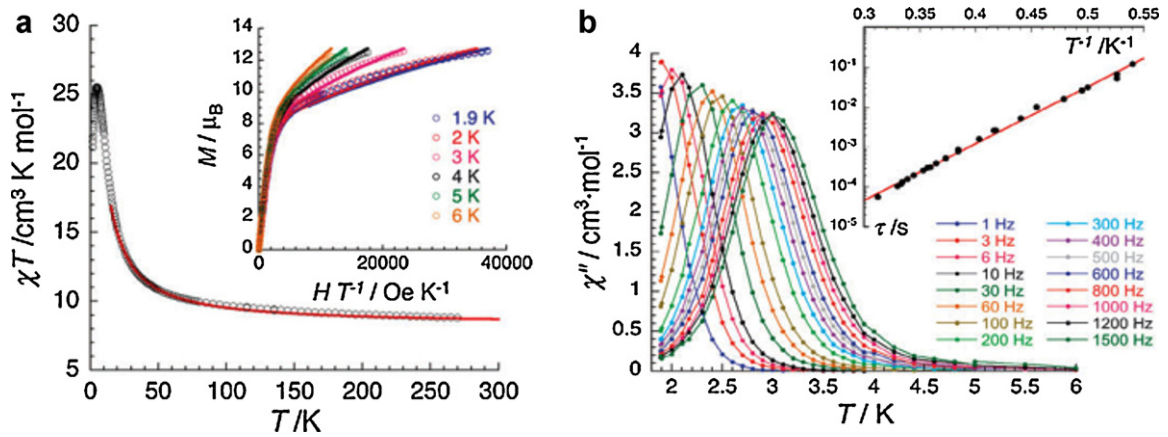

Fig. 16. (a) χT vs T data for $[(Tp^{*Me})_4Fe^{III}(CN)_3]_4[Ni^{II}(tren)_4]_4(ClO_4)_4{\cdot}7H_2O{\cdot}4MeCN$ at $H = 0.1T$ (with χ defined as the molar magnetic susceptibility equal to M/H). Inset: magnetization vs H/T between 1.9 and 6 K. Solid lines represent least-squares fitting of the data to anisotropic $S_T = 6$ macro-spin model. (b) χ'' vs T data below 6 K at various ac frequencies ($H = 0$ Oe; $H = 3$ Oe). Inset: semi-logarithmic τ vs T^{-1}. Red solid line is the best simulation of data using an Arrhenius law (with $\tau_0 = 2.5 \times 10^{-9}$ s). Reprinted with permission from Ref. [70]. Copyright 2010 The Royal Society of Chemistry.

a square pyramidal $Cu(NC)_4(H_2O)$ coordination sphere. All of the cyanide bridges deviate somewhat from strict linearity, as reflected in the Fe–C≡N and Cu–N≡C angles, which are distributed within the range 171.3(6)–177.6(6)°. The C≡N stretching region in the infrared spectrum is consistent with the presence of only bridging cyanide ligands (a peak of medium intensity at 2176 cm^{-1}) and the high symmetry of the structure. In all, the cluster closely approaches cubic (O_h) symmetry, with Fe···Fe cube edge distances in the range 6.827–6.938 Å and crystallographically imposed Fe···Fe···Fe angles of 90°.

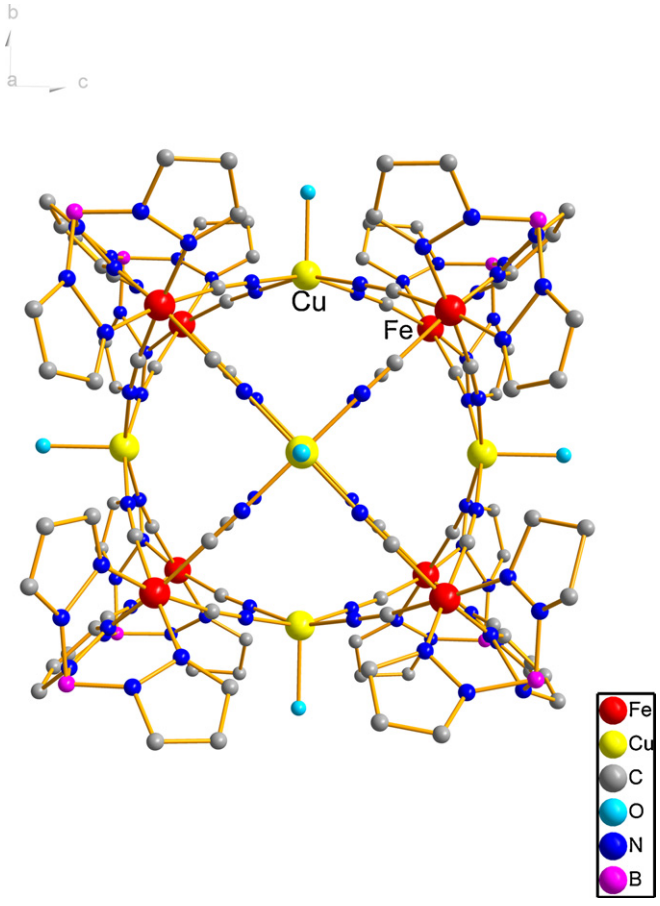

Fig. 17. View of the molecular structure of the fourteen-nuclear complex $[(Tp)_8(H_2O)_6Cu_6Fe_8(CN)_{24}](ClO_4)_4{\cdot}12H_2O{\cdot}2Et_2O$. The anions and the solvate molecules have been removed for clarity [71].

Importantly, the Fe_8Cu_6 cluster represents the first structurally characterized example of a face-centered cubic cluster in which both metal sites are occupied by paramagnetic ions. Magnetic studies revealed the expected ferromagnetic interactions between the orthogonal spin orbitals of the Fe^{III} and Cu^{II} ions ($J_{FeCu} = +15\ cm^{-1}$), resulting in an $S = 7$ ground state. Despite its cubic symmetry, least-squares fitting of the M vs H/T data affords zero-field splitting parameters of $D = -0.16\ cm^{-1}$, suggesting that the maximum energy barrier is 7.8 cm^{-1}. Frequency-dependent χ''_M signals were observed below 3 K, indicating the superparamagnet-like slow relaxation of a SMM.

Reactions between $[TpFe(CN)_3]^-$ and $M(ClO_4){\cdot}6H_2O$ (M = Co and Ni) in a mixture of acetonitrile and methanol afford, upon crystallization via THF vapor diffusion, $[Tp(H_2O)_{12}M_6Fe_8(CN)_{24}](ClO_4)_4{\cdot}12THF{\cdot}4H_2O$ (M = Co and Ni) [72]. Both compounds contain cyano-bridged clusters with a similar face-centered cubic geometry, wherein octahedral Co or Ni centers are situated at the face-centering sites. The results of variable-temperature magnetic susceptibility measurements indicate the presence of ferromagnetic exchange coupling within both molecules to give ground states of $S = 10$ and 7, respectively. Low-temperature magnetization data reveal significant zero-field splitting, with the best fits for the Fe_8Co_6 and Fe_8Ni_6 clusters yielding $D = -0.54$ and 0.21 cm^{-1}, respectively. No evidence of the slow relaxation effects associated with SMM behavior was observed. Long and co-workers have shown that the utility of the $S = 3/2$ tricyanometalate precursor, $[TpCr(CN)_3]^-$, in generating HS face-centered cubic cluster $[Tp(H_2O)_6Cu_6Cr_8(CN)_{24}](ClO_4)_4{\cdot}12THF{\cdot}4H_2O$ (orange crystals) and $[Tp(H_2O)_6Cu_6Cr_8(CN)_{24}](ClO_4)_4{\cdot}13THF{\cdot}15H_2O$ (green crystals) [28]. Evidence for cyanide ligand reorientation in $[Tp(H_2O)_6Cu_6Cr_8(CN)_{24}](ClO_4)_4{\cdot}12THF{\cdot}4H_2O$ has been confirmed by structural and spectroscopic analyses. The asymmetric unit consists of both Cr–CN–Cu and Cr–NC–Cu linkages. Magnetic studies indicate the presence of ferromagnetic exchange coupling for both samples, as expected for cyanide bridges between octahedral Cr^{III} (t_{2g}^3) and square pyramidal Cu^{II} (b_{1g}) centers. Low-temperature

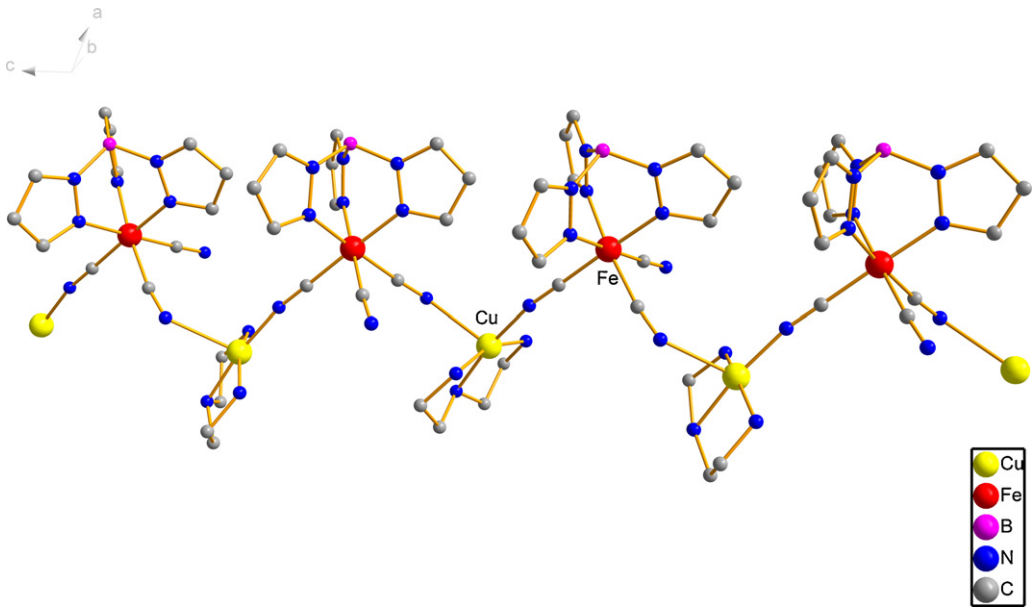

Fig. 18. View of the 2,2-*CC* chain $[(Tp)Fe^{III}(CN)_3Cu(dien)]ClO_4{\cdot}H_2O$. The anions and the solvate molecules have been removed for clarity [44].

magnetization data confirm the HS ground states ($S = 15$) with negligible zero-field splitting. Consistent with the apparent lack of magnetic anisotropy, no out-of-phase signal was observed for either sample.

4. One-dimensional assemblies

Self-assembly of the anionic building block, *fac* or *mer*-$[LFe(CN)_3]^-$ and metal ions in the presence (or absence) of blocking ligands have frequently resulted in the formation of chains with different topologies: (i) Fe^{III}–Cu^{II} 2,4-ribbon: $[(Tp)_2Fe^{III}_2(CN)_6Cu^{II}(CH_3OH){\cdot}2CH_3OH]_n$ [73], $[(bpca)_2Fe^{III}_2(CN)_6Cu^{II}(H_2O)_2{\cdot}1.5H_2O]_n$ [48], Fe^{III}–Mn^{II} 2,4-ribbon: $\{([Tp)Fe^{III}(CN)_3]_2Mn^{II}(DMF)_2\}_n$ [74], Fe^{III}–Fe^{II} 2,4-ribbon: $[Fe^{III}(Tp)\ (CN)_3]_4Fe^{II}(H_2O)_2Fe^{II}$ [64], $[Fe^{II}Fe^{III}_2(CN)_6(tp^*)_2(DMF)]{\cdot}2DMF{\cdot}H_2O$ [75]; (ii) Fe^{III}–Mn^{II} 3,3-ladder: $\{[Fe^{III}(bpca)(\mu\text{-}CN)_3]Mn^{II}(H_2O)_3\}[Fe^{III}(bpca)(CN)_3]{\cdot}3H_2O$ [32]; (iii) Fe^{II}–Mn^{II} 2,2-*CT* (*C* = *Cis*; *T* = *Trans*) chain: $[Fe^{II}(Tpms)(CN)_3][Mn^{II}(H_2O)_2(DMF)_2]{\cdot}DMF$ [76], Fe^{III}–Mn^{III} 2,2-*CT* chains: $[(Tp)Fe^{III}(CN)_3Mn^{III}(5\text{-}MeOsalen){\cdot}2CH_3OH]_n$ (5-MeOsalen = N,N′-ethylenebis(5-methoxysalicylideneiminate) [77], $[(PzTp)Fe(CN)_3Mn(5\text{-}MeOsalen){\cdot}CH_3CN]_n$ [78], $[Fe(pzcq)(CN)_3][Mn(salen)]{\cdot}4H_2O$ [33], $[Fe(mpzcq)(CN)_3][Mn(salcy)]{\cdot}MeOH{\cdot}MeCN$ (salcy = N,N′-(trans-1,2-cyclohexanediylethylene)bis-(salicylideneiminato) dianion) [34], $[Fe(qcq)(CN)_3][Mn(5\text{-}Clsalen)]{\cdot}2MeOH$, $[Fe(qcq)(CN)_3][Mn(5\text{-}Brsalen)]{\cdot}2MeOH$ 5-Brsalen = N,N′-ethylenebis(5-bromosalicylideneiminato) dianion, $[Fe(qcq)(CN)_3][Mn(salen)]{\cdot}MeCN$ [36]; (iv) Fe^{III}–Cu^{II} 2,2-*CC* chain $[(Tp)Fe^{III}(CN)_3Cu(dien)]ClO_4{\cdot}H_2O$ (dien = diethylenetriamine) [44] and a Fe^{III}–Cu^{II} chiral helical chain $[(bpca)Fe^{III}(CN)_3Cu^{II}(bpca)(H_2O){\cdot}H_2O]_n$ [48]; (v) Fe^{III}–Ni^{II} zigzag chain $[Fe^{III}\{HB(pz)_3\}(CN)_3]_2[Ni^{II}(dpt)]_n{\cdot}3nH_2O$ ($HB(pz)_3$ = hydrotris(1-pyrazolyl)borate, dpt = dipropylenetriamine) [79], Fe^{III}–Ni^{II} enantiomeric 3,2-chains $\{[(Tp)_2Fe_2(CN)_6Ni_3((1S,2S)\text{-}chxn)_6](ClO_4)_4{\cdot}2H_2O\}_n$ and $\{[(Tp)_2Fe_2(CN)_6Ni_3((1R,2R)\text{-}chxn)_6](ClO_4)_4{\cdot}2H_2O\}_n$ [50].

The first 1D network based on the *fac*-tricyanometalate anionic precursor, $[(Tp)Fe^{III}(CN)_3Cu(dien)]ClO_4{\cdot}H_2O$, was in 2004 [44]. The reaction of $Cu(ClO_4)_2{\cdot}6H_2O$, dien and $(NBu_4)[(Tp)Fe(CN)_3]$ in aqueous solution leads to the formation of a 1D cationic polymer $\{[TpFe(CN)_3][Cu(dien)]\}_n{}^{n+}$, with free perchlorate as counteranions. The 2,2-*CC* chain is made up of a cyano-bridged alternating $[TpFe(CN)_3]^-$–$[Cu(dien)]^{2+}$ fragment (Fig. 18). Within the chain, $[TpFe(CN)_3]^-$ uses two *cis*-CN groups to connect with two $[Cu(dien)]^{2+}$ units, while each $[Cu(dien)]^{2+}$ unit is linked to two $[TpFe(CN)_3]^-$ ions at *cis* positions. Each Cu(II) center adopts a distorted square pyramidal geometry, where one $[TpFe(CN)_3]^-$ unit is bound to the basal site, the other is bound to the elongated apical site and the remaining three basal sites are occupied by the dien ligand. Attempts to use the *mer*-$[(bpca)Fe^{III}(CN)_3]^-$ tricyanometalate precursor and other tridentate blocking ligands have resulted in the formation of a similar chiral helical chain $[(bpca)Fe^{III}(CN)_3Cu^{II}(bpca)(H_2O){\cdot}H_2O]_n$ [48].

The magnetic susceptibility data for the complex $[(Tp)Fe^{III}(CN)_3Cu(dien)]ClO_4{\cdot}H_2O$ revealed ferromagnetic interactions between the Fe(III) and Cu(II). The 1D chain was considered as alternating uniform Fe-Cu dimers with the intradimeric ($J_{FeCu} = +10.9\,cm^{-1}$) and interdimeric exchange constants ($J_{FeCu} = +1.29\,cm^{-1}$). The small interdimeric exchange constants value has been attributed to the more bent Cu–N≡C bond angle (138.1(3)°), which has an unfavorable effect on the magnetic coupling. No long-range ordering was detected down to 2 K. This result is in agreement with those reported for the helical chain $[(bpca)Fe^{III}(CN)_3Cu^{II}(bpca)(H_2O){\cdot}H_2O]_n$ [48].

The reaction of $Cu(NO_3)_2{\cdot}6H_2O$ and *fac*-$[(Tp)Fe(CN)_3]^-$ in the molar ratio 1:2 in the mixture of water and methanol solution affords the complex $[(Tp)_2Fe^{III}_2(CN)_6Cu(CH_3OH){\cdot}2CH_3OH]_n$ [73]. X-ray crystallographic analysis reveals the formation of 2,4-ribbon like chains of squares. The basic structural unit is a $Cu_2(CN)_4Fe_2$ square with each Cu^{II} shared by two adjacent squares (Fig. 19). Within each square, the $[(Tp)Fe(CN)_3]^-$ unit binds two Cu^{II} through two of its three cyanide groups. The copper atom is penta-coordinated, with a distorted square-pyramidal geometry. The basal positions are occupied by four cyanide nitrogen atoms, while the apical position is occupied by an oxygen from a methanol molecule. The Cu–N≡C bond angles are 167.4(3)–179.3(3)°. The Cu–N bonds (average length 1.968(3) Å) are shorter than the Cu–O bond (2.232(3) Å). The average intrachain Cu···Fe, Cu···Cu and Fe···Fe separations are 5.018, 6.782, and 6.782 Å, respectively. Whereas, the shortest intermolecular Cu···Cu, Cu···Fe, and Fe···Fe distance are

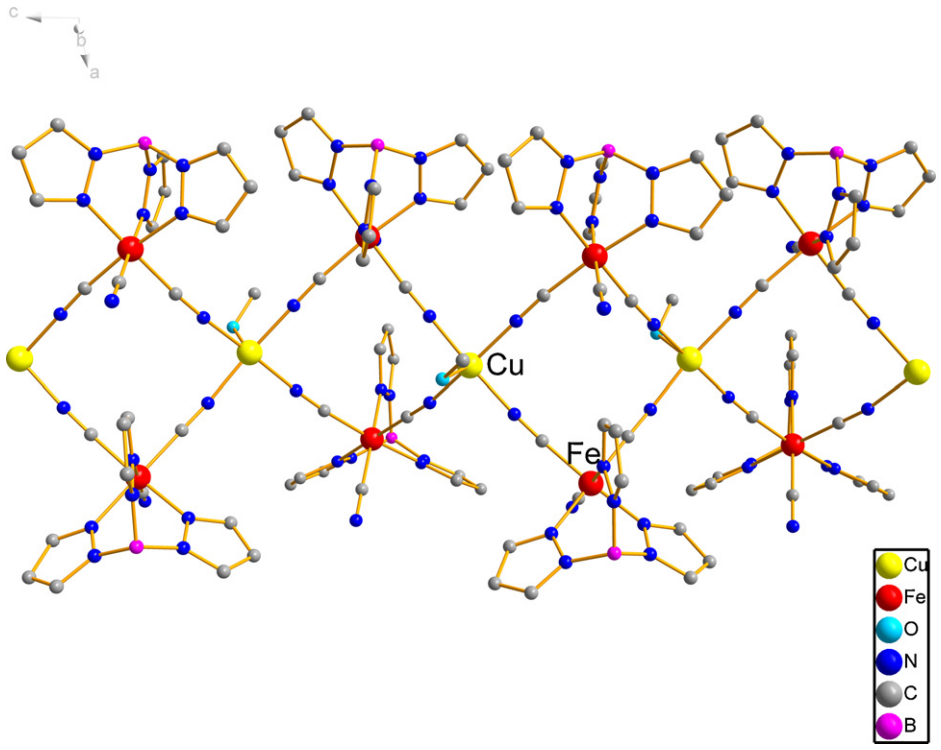

Fig. 19. View of the 2,4-ribbon like chain $[(Tp)_2Fe^{III}{}_2(CN)_6Cu(CH_3OH)\cdot 2CH_3OH]_n$. The solvate methanol molecules have been removed for clarity [73].

11.100, 8.813, and 8.448 Å, respectively. Similar structures have been reported for $[(bpca)_2Fe^{III}{}_2(CN)_6Cu^{II}(H_2O)_2\cdot 1.5H_2O]_n$ [48] and $\{([Tp)Fe^{III}(CN)_3]_2Mn^{II}(DMF)_2\}_n$ [74].

For $[(Tp)_2Fe^{III}{}_2(CN)_6Cu^{II}(CH_3OH)\cdot 2CH_3OH]_n$, magnetic susceptibility data revealed the intrachain ferromagnetic interaction between the Fe^{III} and Cu^{II} ions ($J_{FeCu} = 32.3\,cm^{-1}$ and $12.3\,cm^{-1}$) and interchain magnetic interactions were not observed down to 1.8 K. Much weaker ferromagnetic coupling ($J_{FeCu} = 10.9\,cm^{-1}$ and $1.29\,cm^{-1}$) was observed in the related $[(Tp)Fe^{III}(CN)_3Cu(dien)]ClO_4\cdot H_2O$ [44] where single cyanide bridges link alternatively LS iron(III) and copper(II) ions. The greater deviation from linearity of the cyanide bridges at the C≡N–Cu fragment in the latter compound [170.4(3)° and 138.1(3)° vs 174.5(3)–178.3(3)° in the 2,4-ribbon like chain] is responsible for its weaker magnetic coupling. The AC magnetic susceptibilities are strongly frequency-dependent below 6 K (Fig. 20). The frequency dependence precludes a three-dimensional ordering. The best set of parameters of an Arrhenius plot is $\tau_0 = 2.8 \times 10^{-13}$ s and $\Delta/k_B = 112.3$ K, suggesting a thermally activated mechanism and superparamagnetic behavior.

A similar structure has been reported for the complex $[(bpca)_2Fe^{III}{}_2(CN)_6Cu^{II}(H_2O)_2\cdot 1.5H_2O]_n$ [48]. Magnetic studies showed metamagnetic behavior with a Neel temperature of $T_N = 2.2$ K and a critical field of 250 Oe at 1.8 K. The cyanides mediate the intrachain ferromagnetic coupling between Cu^{II} and Fe^{III} ions. The Cu^{II} ions are six-coordinated in an elongated distorted octahedral environment. There exist hydrogen bonds and short intermolecular contacts between the adjacent chains. In the case of the chain $\{([Tp)Fe^{III}(CN)_3]_2Mn^{II}(DMF)_2\}_n$, a weak antiferromagnetic coupling between the Fe(III) and Mn(II) ions is observed and it displays also a metamagnetic-like behavior with $T_N = 5.2$ K and $H_C = 10.5$ kOe [74].

Recently, Oshio and co-workers reported a new mixed-valence $Fe^{III}Fe^{II}$ cyano-bridged chain, $[Fe^{II}Fe^{III}{}_2(CN)_6(tp^*)_2(DMF)]\cdot 2DMF\cdot H_2O$, with a similar 2,4-ribbon geometry [75]. Weak antiferromagnetic intrachain interactions and/or orbital contribution from LS Fe^{III} and HS Fe^{II} ions were observed, which lead a spin alignment with $S = 1$ units. AC magnetic susceptibility measurements reveal both a frequency-dependent out-of-phase and in-phase signal suggestive of SCM behavior. The best set of parameters of an Arrhenius plot is $\tau_0 = 2.31 \times 10^{-10}$ s and $\Delta/k_B = 71.7$ K, with the blocking temperature $T_B = 2.7$ K. Magnetic hysteresis measurement for aligned single crystals at low temperature (1.8 K) indicates that the anisotropic easy axis is arbitrary perpendicular to the chain (*b*-axis).

The first 1D complex build from the *mer*-$[LFe(CN)_3]^-$, $\{[Fe^{III}(bpca)(\mu\text{-}CN)_3]Mn^{II}(H_2O)_3\}[Fe^{III}(bpca)(CN)_3]\cdot 3H_2O$, has been reported by Julve and co-workers [32]. The crystallographic analysis revealed an anionic salt made up of cationic 3,3-ladder like chain, $\{[Fe^{III}(bpca)(\mu\text{-}CN)_3]Mn^{II}(H_2O)_3\}^+$, uncoordinated anion $[(bpca)Fe^{III}(CN)_3]^-$ and crystallization water molecules (Fig. 21). In the cationic chain, $[(bpca)Fe^{III}(CN)_3]^-$ acts as a tris-monodentate ligand through its three cyanide groups toward three manganese atoms. The iron atoms exhibit the FeN_3C_3 distorted octahedral environment. The main distortion at the iron atom arises from the geometric constraints caused by the two five-membered chelate rings which are subtended by the tridentate bpca ligand. The manganese atom has a distorted MnN_3O_3 octahedral geometry with the three cyanide-nitrogen atoms in *mer*-position. An extensive network of hydrogen bonds involving the cationic chain, the uncoordinated anions $[(bpca)Fe^{III}(CN)_3]^-$ and crystallization water molecules lead to a three-dimensional structure. The magnetic studies confirm a ferrimagnetic chain with significant intrachain antiferromagnetic coupling between the LS Fe(III) centers and the HS Mn(II) cations and it exhibits ferrimagnetic ordering below 2.0 K.

Attempts to extend this work to other anisotropic ions such as manganese(III), afforded a series of Fe^{III}–Mn^{III} 2,2-*CT* chains: $[(Tp)Fe^{III}(CN)_3Mn^{III}(5\text{-}MeOsalen)\cdot 2CH_3OH]_n$ [77], $[(PzTp)Fe(CN)_3Mn(5\text{-}MeOsalen)\cdot CH_3CN]_n$ [78], $[Fe(pzcq)(CN)_3][Mn(salen)]\cdot 4H_2O$ [33], $[Fe(mpzcq)(CN)_3][Mn(salcy)]\cdot MeOH\cdot MeCN$ [34],

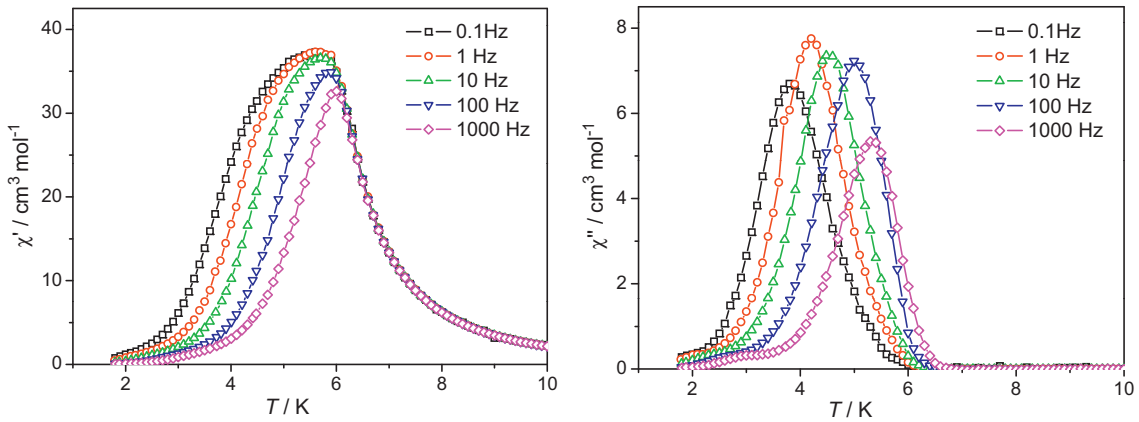

Fig. 20. Temperature dependence of the in-phase and out-of-phase components of the *ac* susceptibility for $[(Tp)_2Fe^{III}{}_2(CN)_6Cu(CH_3OH)\cdot 2CH_3OH]_n$ in zero applied static field with an oscillating field 5 Oe in frequency of 0.1–1000 Hz [73].

[Fe(qcq)(CN)$_3$][Mn(5-Clsalen)]·2MeOH, [Fe(qcq)(CN)$_3$][Mn(5-Brsalen)]·2MeOH and [Fe(qcq)(CN)$_3$][Mn(salen)]·MeCN [36]. In general, the Fe^{III}–Mn^{III} chain are obtained by stoichiometric reaction of *fac*- or *mer*-$[LFe(CN)_3]^-$ and Mn(III) Schiff base complex cation in organic solvent. In the complex $[(Tp)Fe^{III}(CN)_3Mn^{III}(5\text{-MeOsalen})\cdot 2CH_3OH]_n$, the structure is made of neutral cyano-bridged 2,2-*CT* like Fe^{III}–Mn^{III} zigzag chains (Fig. 22). The zigzag pattern is determined by the *cis* topology of bridges emerging from $[TpFe(CN)_3]^-$. The manganese ion is six-coordinated in an elongated octahedral geometry (formally, a Jahn–Teller distortion). The equatorial plane is occupied by N_2O_2 donor atoms of 5-MeOsalen, whereas two other cyanide nitrogen atoms occupy the axial positions. The chain shows two alternating types of Fe–C≡N–Mn bridges, labeled here a and b, closely similar in bond lengths, e.g. $(Mn–N)_a = 2.364(2)$ Å, $(Mn–N)_b = 2.320(2)$ Å, but having different bond and dihedral angles, like $(C{\equiv}N–Mn)_a = 161.7(2)^\circ$ vs $(C{\equiv}N–Mn)_b = 151.1(2)^\circ$, $(Fe–C{\equiv}N–Mn)_a = 23.7^\circ$ vs $(Fe–C{\equiv}N–Mn)_b = 158.2^\circ$.

The $\chi_M T$ curve has a ferromagnetic main pattern and antiferromagnetic trend at lower temperature (Fig. 23a). The magnetic susceptibility measurements agree with ferromagnetic interaction between the Fe(III) and Mn(III) ions ($J_{FeMna} = 1.66\ cm^{-1}$ and $J_{FeMnb} = 1.21\ cm^{-1}$). At low temperatures, a magnetic susceptibility maximum is observed at 4.8 K for low fields, which broadens as the magnetic field increases and disappears for $H > 3500$ G, proving a field-induced transition from antiferromagnetic to a ferromagnetic ground state (Fig. 23b). The steep decrease in $\chi_M T$ at low temperature is due to the interchain antiferromagnetic coupling. The interchain Ising-like resonant interaction model was used to confirm the interchain antiferromagnetic coupling ($zJ = -0.038\ cm^{-1}$) which causes the metamagnetic behavior with loss of magnetization relaxation effects. The AC magnetic susceptibility shows zero out-of-phase signals and no frequency-dependent behavior was observed. The metamagnetic behavior of this compound is further evident from the sigmoidal shape of the *M* vs *H* plot at 1.8 K and the fast increase of *M* at *H* about 3500 G. (Fig. 23b). Under an applied field greater than 3500 G, the interchain antiferromagnetic coupling is overcome. The *M* vs *H* curve has the behavior expected for a metamagnet with a large anisotropy.

Broken symmetry DFT calculations were performed on the heterodinuclear single cyano-bridged *a* and *b* {FeMn} dimer moieties taken from the experimental geometries lead to $J_{FeMna} = 2.4\ cm^{-1}$

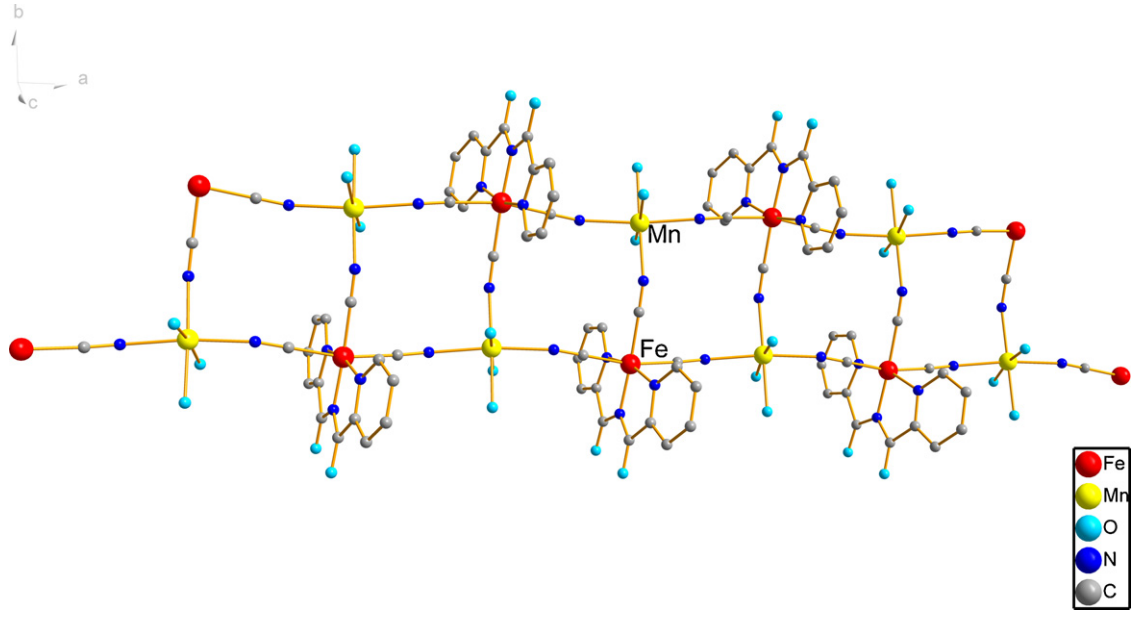

Fig. 21. View of the 3,3-ladder like chain $\{[Fe^{III}(bpca)(\mu\text{-}CN)_3]Mn^{II}(H_2O)_3\}[Fe^{III}(bpca)(CN)_3]\cdot 3H_2O$. The uncoordinated anions $[(bpca)Fe^{III}(CN)_3]^-$ and crystallization water molecules have been removed for clarity [32].

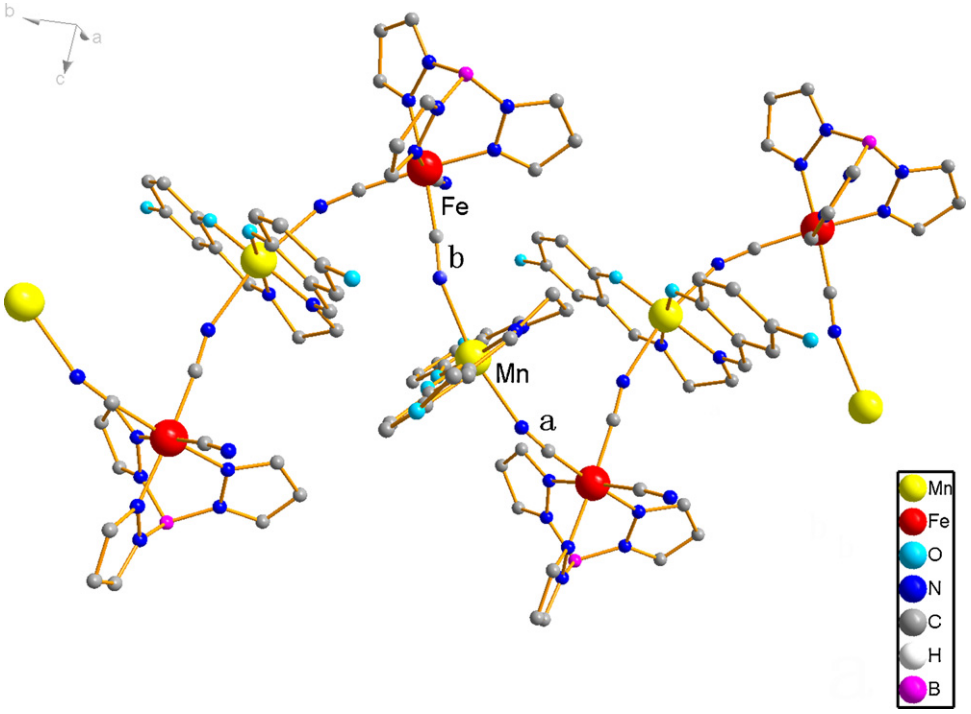

Fig. 22. View of the 2,2-*CT* like zigzag chain $[(Tp)Fe^{III}(CN)_3Mn^{III}(5\text{-MeOsalen})\cdot 2CH_3OH]_n$. The crystallization methanol molecules have been removed for clarity [77].

and $J_{FeMnb} = 1.7\ cm^{-1}$ estimations, which are consistent with the range and sign of the experimental fitting values. Much stronger ferromagnetic coupling ($J_{FeMn} = 4.05\ cm^{-1}$) was observed in the related $[(PzTp)Fe(CN)_3Mn(5\text{-MeOsalen})\cdot CH_3CN]_n$ [78], which differs in the outer substituent (non coordinating pyrazolato in PzTp instead of H in Tp). The slight change of the Mn(III) coordination sites is responsible for its stronger magnetic coupling and weaker interchain magnetic coupling ($zJ = -0.02\ cm^{-1}$).

Hong and co-workers have shown that the use of *mer*-$[LFe(CN)_3]^-$ building blocks and Mn(III) salen type complexes is an alternative synthetic route for the design of similar cyano-bridged 2,2-*CT* like Fe^{III}–Mn^{III} zigzag chains: $[Fe(pzcq)(CN)_3][Mn(salen)]\cdot 4H_2O$ [33], $[Fe(mpzcq)(CN)_3][Mn(salcy)]\cdot MeOH\cdot MeCN$ [34], $[Fe(qcq)(CN)_3][Mn(5\text{-Clsalen})]\cdot 2MeOH$, $[Fe(qcq)(CN)_3][Mn(5\text{-Brsalen})]\cdot 2MeOH$ and $[Fe(qcq)(CN)_3][Mn(salen)]\cdot MeCN$ [36]. In general, all complexes consist of extensive hydrogen bonding and stacking interactions coming from the planes of the ligand, generating multidimensional structures. In contrast to ferromagnetic interactions observed in the Fe^{III}–Mn^{III} chain formed by the *fac*-$[TpFe(CN)_3]^-$ anion discussed above, the magnetic susceptibility data revealed intrachain antiferromagnetic interactions between Fe(III) and Mn(III) (J_{FeMn} in the range of -3.3 to $-8.6\ cm^{-1}$) and weak interchain antiferromagnetic interactions in these complexes. The nature of magnetic coupling between Fe(III) and Mn(III) ions via the CN bridges is consistent with the Fe–Mn systems made of *mer*-Fe tricyanides. It appears that the Fe–CN–Mn unit can provide either antiferromagnetic or ferromagnetic coupling depending on the subtle structural variations present in bridging pathways. Magnetic studies demonstrate that a field-induced metamagnetic transition is observed in $[Fe(mpzcq)(CN)_3][Mn(salcy)]\cdot MeOH\cdot MeCN$ [34]. A long-range order is observed at about 2 K for $[Fe(qcq)(CN)_3][Mn(5\text{-Clsalen})]\cdot 2MeOH$ and $[Fe(qcq)(CN)_3][Mn(5\text{-Brsalen})]\cdot 2MeOH$, while compound $[Fe(qcq)(CN)_3][Mn(salen)]\cdot MeCN$ shows spin glass behavior coupled with magnetic ordering [36].

When extending this work to the anisotropic ions such as nickel(II), Julve and co-workers reported a new type of cyano-bridged zig-zag chain complex, $[Fe^{III}\{HB(pz)_3\}(CN)_3]_2[Ni^{II}(dpt)]_n\cdot 3nH_2O$ [79]. The chain consists of regular alternating bis-monodentate $[Fe\{HB(pz)_3\}(CN)_3]^-$

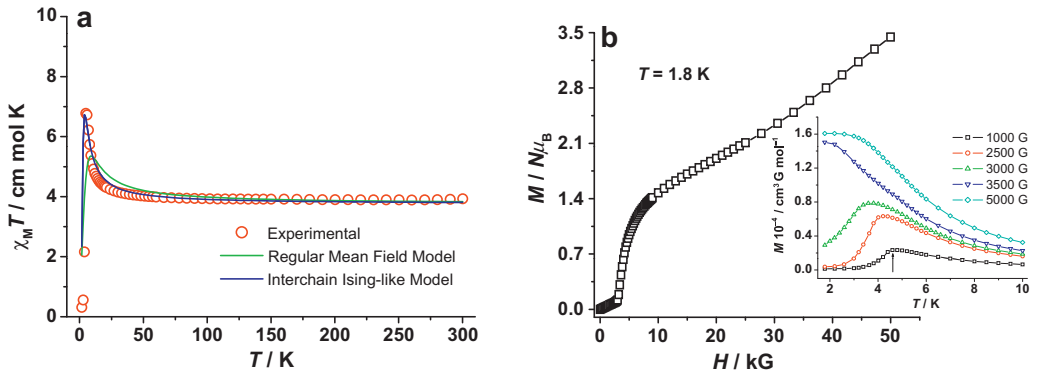

Fig. 23. (a) The $\chi_M T$ vs T for $[(Tp)Fe^{III}(CN)_3Mn^{III}(5\text{-MeOsalen})\cdot 2CH_3OH]_n$. Solids lines: the fit with different interchain models. (b) Field dependence of the magnetization at 1.8 K. Lower inset: field-cooled magnetization at different applied fields [77].

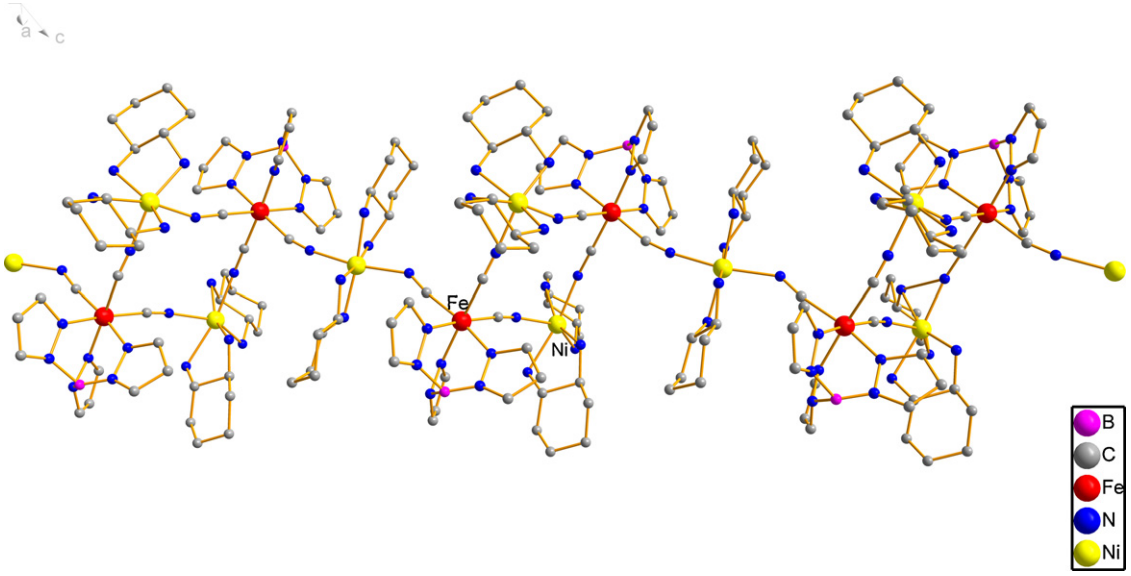

Fig. 24. View of the chiral 3,2-chain $\{[(Tp)_2Fe_2(CN)_6Ni_3((1S,2S)\text{-chxn})_6](ClO_4)_4\cdot 2H_2O\}_n$. The perchlorate anions and crystallization water molecules have been removed for clarity [50].

units and $[Ni(dpt)]^{2+}$ cations, the six coordination geometry around the nickel atom is achieved by the coordination of another $[Fe\{HB(pz)_3\}(CN)_3]^-$ group acting as a monodentate end-cap ligand. Magnetic data show the occurrence of intrachain ferromagnetic coupling ($J = +5.7\ cm^{-1}$) and metamagnetic behavior with the critical field being $H_c = 700$ Oe. The metamagnetic behavior is due to the existence of weak interchain antiferromagnetic interactions ($J = 0.07\ cm^{-1}$). The incipient frequency dependence of the out-of-phase signal under applied dc field $H > H_c$ is observed at $T < 4.5$ K. The occurrence of a slow relaxation of the magnetization is reminiscent of the SCM behavior.

The reaction of $Ni(ClO_4)_2\cdot 6H_2O$ with $(NBu_4)[TpFe(CN)_3]$ and (1S,2S)-(+)-1,2-diaminocyclohexane (or (1R,2R)-1,2-diaminocyclohexane) in a mixture of water, methanol and acetonitrile results in the formation of two new cyano-bridged heterobimetallic 1D complexes, $\{[(Tp)_2Fe_2(CN)_6Ni_3((1S,2S)\text{-chxn})_6](ClO_4)_4\cdot 2H_2O\}_n$ and $\{[(Tp)_2Fe_2(CN)_6Ni_3((1R,2R)\text{-chxn})_6](ClO_4)_4\cdot 2H_2O\}_n$ [50]. X-ray crystallography reveals that they are enantiomers and crystallized in the chiral space group (P_1). The structure consists of a novel 1D heterobimetallic cationic 3,2-chain formed by alternating arrays of $\{(Tp)Fe(CN)_3Ni[(1S,2S)\text{-chxn}]_2\}_2^{2+}$ square and *trans*-$\{Ni[(1S,2S)\text{-chxn}]_2\}^{2+}$ fragments bridged by cyanide groups along *b* axis (Fig. 24), with free perchlorate counter anions. Despite its large structural distortion, the size of the Fe_2Ni_2 square unit is in agreement with those of cyano-bridged Fe_2Ni_2 square clusters reported previously [29,53–56]. The 1D chains are further linked through hydrogen bonds between perchlorate anions and (1S,2S)-chxn ligands.

DC magnetic studies show ferromagnetic coupling between the orthogonal spin orbitals of Fe^{III} and Ni^{II}, resulting in $S = 4$ ground state, which is further confirmed by the unsaturated magnetization value of $7.42\mu_B$ under the 7 T magnetic field at 1.8 K. The magnetic susceptibility is field dependent at temperatures lower than 3 K. A maximum of susceptibility appears at ca. 2.5 K under $H \leq 2$ kOe, and this maximum disappears for $H > 5$ kOe, suggesting that a field-induced transition from an antiferromagnetic to a ferromagnetic ground state occurs below 3 K (Fig. 25a). However, the AC magnetic susceptibilities are strongly frequency-dependent below 5 K. The frequency dependence precludes a three-dimensional ordering. The best set of parameters of an Arrhenius plot is $\tau_0 = 4.4 \times 10^{-8}$ s and $\Delta E_{eff} = 19.5$ K, reveal a thermally activated mechanism and the existence of slow magnetization relaxation (Fig. 25b). Furthermore, this complex displays a ferroelectric hysteresis loop, with a coercive field (E_c) of ca. 7.5 kV cm^{-1} and a remnant polarization (P_r) of 0.10 μc cm^{-1}. They are the first example of multiferroic compounds bearing both slow magnetization relaxation and ferroelectricity [50].

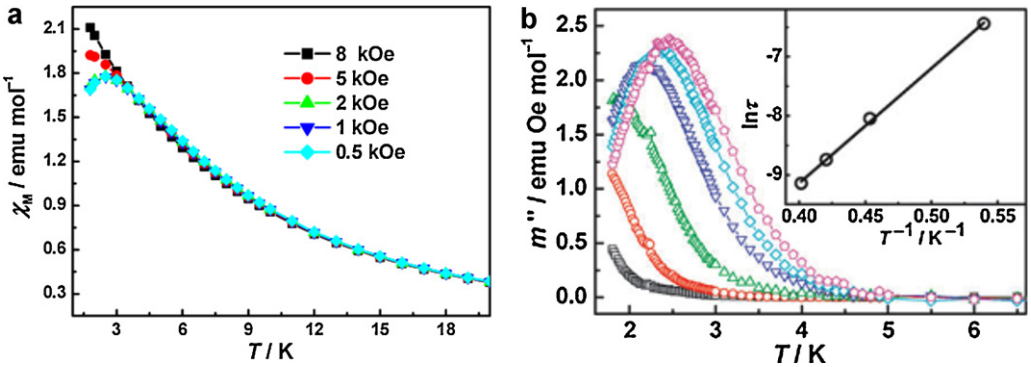

Fig. 25. (a) Field dependence of the magnetic susceptibility of $\{[(Tp)_2Fe_2(CN)_6Ni_3((1S,2S)\text{-chxn})_6](ClO_4)_4\cdot 2H_2O\}_n$ at very low temperatures. (b) Out-of-phase component of the AC magnetization data, recorded with switching frequencies of 1 (□), 10 (○), 100 (△), 500 (▽), 1000 (◇), and 1488 (⌂) Hz. Inset: Arrhenius law fit of peak maximum as a function of relaxation time [50].

Table 1
Some of the reported cyano-bridged Fe(III)–M(II) compounds and their *J* values.

	Metal	*g*	*J* (cm^{-1})[a]	Ref.
Dinuclear cyano-bridged complexes				
$[Fe(pzcq)(CN)_3][Mn(phen)_2(Cl)]\cdot MeOH$	Fe^{III}–Mn^{II}	2.03	−3.32	[39]
$[Fe(pzcq)(CN)_3][Mn(phen)_2(Br)]\cdot MeOH$	Fe^{III}–Mn^{II}	2.03	−3.69	[39]
$[Fe(mpzcq)(CN)_3][Mn(phen)_2(Cl)]\cdot MeOH$	Fe^{III}–Mn^{II}	1.99	−2.23	[39]
$[(Tp)Fe(CN)_3Cu(bipy)_2]\cdot ClO_4\cdot CH_3OH$	Fe^{III}–Cu^{II}	2.34	5.52	[40]
fac-$\{[Fe^{III}(pzTp)(CN)_2(\mu\text{-}CN)]\ Cu^{II}(TPyA)\}\cdot Et_2O\cdot ClO_4$	Fe^{III}–Cu^{II}	2.01	11.55	[41]
$[(Tp)Fe(CN)_3][Mn(1\text{-}napen)(H_2O)]\cdot MeCN\cdot 4H_2O$	Fe^{III}–Mn^{III}	2.19	3.74	[43]
$[(Tp)Fe(CN)_3][Mn(5\text{-}Clsalen)(H_2O)]$	Fe^{III}–Mn^{III}	2.2	3.33	[43]
$[(Tp)Fe(CN)_3][Mn(2\text{-}acnapen)(MeOH)]\cdot MeOH$,	Fe^{III}–Mn^{III}	1.98	2.5	[43]
$[Fe(mpzcq)(CN)_3][Mn(salen)(H_2O)]\cdot H_2O$	Fe^{III}–Mn^{III}	2.08	−8.6	[34]
$[Fe(qcq)(CN)_3][Mn(3\text{-}MeOsalen)(H_2O)]\cdot 2H_2O$	Fe^{III}–Mn^{III}	1.96	−4.65	[36]
Trinuclear cyano-bridged complexes				
$[(Tp)_2Fe_2(CN)_6Mn(CH_3OH)_4]\cdot 2CH_3OH$	Fe^{III}–Mn^{II}	2.13	−2.19	[44]
$[(Tp)_2Fe_2(CN)_6Mn(C_2H_5OH)_4]\cdot 2C_2H_5OH$	Fe^{III}–Mn^{II}	2.05	−1.37	[46]
$[(Tp)_2Fe_2(CN)_6Mn(phen)_2]\cdot 5H_2O$	Fe^{III}–Mn^{II}	2.10	−2.29	[47]
$[(bpca)_2Fe_2(CN)_6Mn(CH_3OH)_2(H_2O)_2]\cdot 2H_2O$	Fe^{III}–Mn^{II}	2.086	−3.28	[48]
$[(pcq)_2Fe_2(CN)_6Mn(CH_3OH)_2(H_2O)_2]\cdot 2H_2O$,	Fe^{III}–Mn^{II}	2.05	−1.11	[49]
$[(pcq)_2Fe_2(CN)_6Mn(bipy)_2]\cdot CH_3OH\cdot 2H_2O$	Fe^{III}–Mn^{II}	2.06	−4.03	[49]
$[(pcq)_2Fe_2(CN)_6Mn(phen)_2]\cdot CH_3OH\cdot 2H_2O$.	Fe^{III}–Mn^{II}	2.05	−3.73	[49]
$[(Tp)_2Fe_2(CN)_6Mn(DMSO)_4]$	Fe^{III}–Mn^{II}	2.08	0.708	[51]
$[(Tp)_2Fe_2(CN)_6Ni(cyclam)]\cdot 2H_2O$	Fe^{III}–Ni^{II}	2.37	17.2	[44]
$[(Tp)_2Fe_2(CN)_6Ni(en)_2]\cdot 2H_2O$	Fe^{III}–Ni^{II}	2.25	1.2	[46]
$[(pzTp)_2Fe_2(CN)_6Ni(L)]\cdot 1/2CH_3OH$ (L = 1,5,8,12-tetraazadodecane)	Fe^{III}–Ni^{II}	2.5	0.9	[28]
$[(pzTp)_2Fe_2(CN)_6Ni(bipy)_2]\cdot 2H_2O$	Fe^{III}–Ni^{II}	2.31	4.86	[28]
$[(Tp)_2Fe_2(CN)_6Ni(DMSO)_4]$	Fe^{III}–Ni^{II}	2.30	2.68	[51]
$\{(MeTp)_2Fe_2(CN)_6Ni[(1R,2R)\text{-}chxn]_2\}$	Fe^{III}–Ni^{II}	2.33	2.58	[50]
$[(Tp)_2Fe_2(CN)_6Cu(DMSO)_4]$	Fe^{III}–Cu^{II}	2.31	6.82	[51]
$[(Tp)_2Fe_2(CN)_6Co(DMSO)_4]$	Fe^{III}–Co^{II}	2.41	−4.91	[51]
Tetranuclear cyano-bridged complexes				
$[Mn_2Fe_2Tp_2(CN)_6(bipy)_2](ClO_4)_2\cdot 4MeCN$	Fe^{III}–Mn^{II}	2.10	−2.29	[45]
$\{[Tp^*Fe(CN)_3Mn(DMF)_4]_2[OTf]_2\}\cdot 2DMF$	Fe^{III}–Mn^{II}	2.1	−2.1	[53]
$\{[Tp^*Fe(CN)_3Co(DMF)_4]_2[OTf]_2\}\cdot 2DMF$	Fe^{III}–Co^{II}	2.7	−10	[53]
$\{[Tp^*Fe(CN)_3Ni(DMF)_4]_2[OTf]_2\}\cdot 2DMF$	Fe^{III}–Ni^{II}	2.2	5.3	[53]
$[TpFe(CN)_3Ni(tren)]_2(ClO_4)_2\cdot 2H_2O$	Fe^{III}–Ni^{II}	2.22	4.52	[54]
$[TpFe(CN)_3Ni(bipy)_2]_2[TpFe(CN)_3]_2\cdot 6H_2O$	Fe^{III}–Ni^{II}	2.67	7.36	[54]
$[(phTp)Fe(CN)_3Ni(tren)]_2(ClO_4)_2$,	Fe^{III}–Ni^{II}	2.284	4.21	[29]
$[(MeTp)Fe(CN)_3Ni(tren)]_2(ClO_4)_2\cdot 2H_2O$	Fe^{III}–Ni^{II}	2.305	2.84	[29]
$[(i\text{BuTp})Fe(CN)_3Ni(tren)]_2(ClO_4)_2\cdot 2H_2O\cdot 2CH_3OH$	Fe^{III}–Ni^{II}	2.285	5.46	[29]
$\{[Tp^*Fe(CN)_3Ni(bipy)_2]_2[OTf]_2\}\cdot 2H_2O$	Fe^{III}–Ni^{II}	2.29	6.5	[55]
$[(pzTp)_2Fe_2Ni_2(dpa)_2(CN)_6](ClO_4)_2\cdot 2CH_3OH\cdot 6H_2O$	Fe^{III}–Ni^{II}	2.23	7.0	[56]
$[TpFe(CN)_3Cu(Tp)]_2\cdot 2H_2O$,	Fe^{III}–Cu^{II}	2.39	11.91	[54]
$[TpFe(CN)_3Cu(bpca)]_2\cdot 4H_2O$,	Fe^{III}–Cu^{II}	2.05	1.38	[54]
$[(phTp)Fe(CN)_3Cu(bipy)(H_2O)(ClO_4)]_2\cdot 2H_2O$,	Fe^{III}–Cu^{II}	2.308	8.90	[29]
$[(Tp)Fe(CN)_3]_2[Mn(acphen)]_2$	Fe^{III}–Mn^{III}	1.98	2.61	[58]
$[(Tp)Fe(CN)_3]_2[Mn(5\text{-}Bracphen)]_2$	Fe^{III}–Mn^{III}	2.02	2.50	[58]
$[(Tp)Fe(CN)_3]_2[Mn(salen)]_2\cdot 6H_2O$	Fe^{III}–Mn^{III}	1.95	−2.15	[58]
Pentanuclear cyano-bridged complexes				
$[(Tp)_3(Tpm(Me))_2(Fe_3Ni_2)(CN)_9]ClO_4\cdot 15H_2O$	Fe^{III}–Ni^{II}	2.27	4.84	[59]
$[(Tp)_2(cyclen)_3Ni_3Fe_2(CN)_6](BF_4)_4$	Fe^{III}–Ni^{II}	2.21	5.4	[62]
$[(Tp)_3(TpmMe)_2(Fe_3Fe_2)(CN)_9]BF_4\cdot 15H_2O$	Fe^{III}–Fe^{II}	2.065	−0.74	[59]
$[(Tp)_2(Me_3tacn)_3Cu_3Fe_2(CN)_6](ClO_4)_4\cdot 2H_2O$,	Fe^{III}–Cu^{II}	2.245	8.5	[60]
$[(Tp^{4Bo})_2(Me_3tacn)_3Cu_3Fe_2(CN)_6](ClO_4)_4\cdot 5H_2O$	Fe^{III}–Cu^{II}	2.28	3.45	[61]
$[(pzTp)_2(Me_3tacn)_3Cu_3Fe_2(CN)_6](ClO_4)_4\cdot 4H_2O$	Fe^{III}–Cu^{II}	2.28	7.92	[61]
Octanuclear cyano-bridged complexes				
$[(pzTp)Fe(CN)_3]_4[NiL]_4[OTF]_4\cdot 10DMF\cdot Et_2O$ (L = 2,2,2-tris(pyrazolyl)ethanol)	Fe^{III}–Ni^{II}	2.20	6.6	[65]
$[(pzTp)Fe(CN)_3]_4[NiL]_4[OTF]_4$ (L = 1-S(Acetyl)-tris(pyrazolyl)hexane)	Fe^{III}–Ni^{II}	2.3	6.6	[66]
$[(pzTp)_4(phen)_4Ni_4Fe_4(CH_3OH)_4(CN)_{12}]_4(ClO_4)_4\cdot 4H_2O$	Fe^{III}–Ni^{II}	2.45	6.0	[61]
$[(Tp^{*Me})_4Fe(CN)_3]_4[Ni(tren)_4]_4(ClO_4)_4\cdot 7H_2O\cdot 4MeCN$	Fe^{III}–Ni^{II}	2.4	6.6	[70]
Fourteen-nuclear cyano-bridged complexes				
$[(Tp)_8(H_2O)_6Cu_6Fe_8(CN)_{24}](ClO_4)_4\cdot 12H_2O\cdot 2Et_2O$	Fe^{III}–Cu^{II}	2.0	15	[71]
One-dimensional complexes				
$[(Tp)_2Fe_2(CN)_6Cu(CH_3OH)\cdot 2CH_3OH]_n$	Fe^{III}–Cu^{II}	2.3	32.3, 12.3	[73]
$[(Tp)Fe(CN)_3Cu(dien)]ClO_4\cdot H_2O$	Fe^{III}–Cu^{II}	2.54	10.9, 1.29	[44]
$[(bpca)Fe(CN)_3Cu(bpca)(H_2O)\cdot H_2O]_n$	Fe^{III}–Cu^{II}	2.196	7.9, 1.03	[48]
$[(Tp)Fe(CN)_3Mn(5\text{-}MeOsalen)\cdot 2CH_3OH]_n$	Fe^{III}–Mn^{III}	2.11	1.66, 1.21	[77]
$[(PzTp)Fe(CN)_3Mn(5\text{-}MeOsalen)]\cdot CH_3CN]_n$	Fe^{III}–Mn^{III}	1.94	4.08	[78]
$[Fe(pzcq)(CN)_3][Mn(salen)]\cdot 4H_2O$	Fe^{III}–Mn^{III}	g_{Mn} = 1.99, g_{Fe} = 2.99	−8.6	[33]
$[Fe(mpzcq)(CN)_3][Mn(salcy)]\cdot MeOH\cdot MeCN$	Fe^{III}–Mn^{III}	g_{Mn} = 1.98, g_{Fe} = 2.08	−3.3	[34]
$[Fe(qcq)(CN)_3][Mn(5\text{-}Clsalen)]\cdot 2MeOH$,	Fe^{III}–Mn^{III}	g_{Mn} = 1.99, g_{Fe} = 2.52	−5.3	[36]
$[Fe(qcq)(CN)_3][Mn(5\text{-}Brsalen)]\cdot 2MeOH$	Fe^{III}–Mn^{III}	g_{Mn} = 1.90, g_{Fe} = 2.48	−5.9	[36]
$[Fe(qcq)(CN)_3][Mn(salen)]\cdot MeCN$	Fe^{III}–Mn^{III}	g_{Mn} = 1.99, g_{Fe} = 2.20	−7.1	[36]
$[Fe\{HB(pz)_3\}(CN)_3]_2[Ni(dpt)]_n\cdot 3nH_2O$	Fe^{III}–Ni^{II}	2.3	5.7	[79]

[a] The data were modeled with the Hamiltonian: such as for the dimer, $H = -2JS_1S_2$ where *J* is the exchange parameter between the Fe^{III} ions and M ion through the cyano-bridges.

5. Conclusions

The present review has outlined the efforts to obtain new magnetic compounds based on the self-assembly reactions between the *fac* or *mer*-$[LFe(CN)_3]^-$ precursors and metal ions in the presence (or absence) of blocking organic ligands and to design new magnetic materials whose nuclearity, topology and magnetic properties can be modulated. The examples presented here illustrate the great variety of structures that can be adopted by the different metal ions and/or organic ligands in the corresponding cyano-bridged assemblies, ranging from di-, tri-, tetra-, penta-, hexa-, oct-, fourteen-nuclear clusters to diverse types of 1D assemblies. Among them, we find the use of *fac*-$[LFe(CN)_3]^-$ as precursors has made possible the achievement of ferromagnetically coupled HS species (including tetra-, penta-, hexa-, oct-, fourteen-nuclear clusters) and a large variety of 1D species exhibiting intramolecular ferro- and antiferro-magnetic coupling. Magnetic data indicate that *fac*- or *mer*-$[LFe(CN)_3]^-$ precursors are ferromagnetic coupled with Ni^{II} and Cu^{II}, antiferromagnetic coupled with Mn^{II} (only one exception) and ferro- or antiferro-magnetic coupled with Co^{II} and Fe^{II} (Table 1). Although *fac*-$[LFe(CN)_3]^-$ mediate ferromagnetic coupling and *mer*-$[LFe(CN)_3]^-$ mediate antiferromagnetic coupling in most of the Fe^{III}–Mn^{III} systems, the geometric parameters relevant to the magnetic Fe–C≡N–Mn pathways are analogous to each other their magnetic natures are varied, which means that a degree of orbital overlap is quite sensitive to a subtle structural change in these systems.

It is not easy to find common features among the nuclearity and topology of this large family of cyano-bridged clusters and 1D complexes, nevertheless, with *mer*-$[LFe(CN)_3]^-$ as precursors, the kinds of structures are limited, it could mean that the shape of the precursor plays an important role in directing the topology of the final crystal structures. Moreover, the slight change in the type of metal ion, the used solvent and/or the organic ligand, transforms the structures of the crystals totally.

Many interesting magnetic properties showed by these complexes are given, such as SMMs, SCMs, multiferroic compounds bearing slow magnetization relaxation and ferroelectricity, thermally induced spin crossover and magnetic optical bistability driven by thermally and photoinduced intramolecular electron transfer. Exploration of tricyanometalate-based molecular assemblies of metal ions possessing large single ion anisotropy, such as Ni^{II}, Mn^{III}, and Co^{II}, has only just begun. Even less is known about this type of chemistry for second- and third-row transition metal ions, for which the increased spin–orbit coupling should be of significant advantage. With the added new topology, related octahedral building units including metal centers such as W^{IV}, Re^{III}, and Re^{v} could be expected to generate even larger anisotropy barriers.

Although the use of tricyanometalate precursors in the cyanide research field has a nearly ten years' period, we believe, in the near future, new metal assemblies with original molecular architectures and new spin topologies will appear. From the crystal engineering point of view, the compounds will provide magnetochemists working in materials science with useful information for further design and investigation on this elusive large family of tricyanometalate-based compounds.

Acknowledgements

The authors gratefully acknowledge financial support from the Natural Science Foundations of China (Grant 20901042), Jiangsu Province (Grants 09KJB150008 and BK2010527) and the National Basic Research Program of China (Grant 2009CB930601). We also thank our co-workers for their distinct contributions and helpful discussions.

References

[1] K.R. Dunbar, R.A. Heintz, Prog. Inorg. Chem. 45 (1997) 283.
[2] M. Verdaguer, A. Bleuzen, V. Marvaud, J. Vaissermann, M. Seuleiman, C. Desplanches, A. Scuiller, C. Train, R. Garde, G. Gelly, C. Lomenech, I. Rosenman, P. Veillet, C. Cartier, F. Villain, Coord. Chem. Rev. 190 (1999) 1023.
[3] M. Ohba, K. Okawa, Coord. Chem. Rev. 198 (2002) 313.
[4] J. Cemark, M. Horendac, I. Potocnak, J. Chomic, A. Horendakova, J. Skorsepa, A. Feher, Coord. Chem. Rev. 224 (2004) 51.
[5] (a) D. William, J. Kouvetakis, M. OflKeefe, Inorg. Chem. 37 (1998) 4617;
(b) M.P. Shores, L.G. Beauvais, J.R. Long, J. Am. Chem. Soc. 121 (1999) 775;
(c) M.P. Shores, L.G. Beauvais, J.R. Long, Inorg. Chem. 38 (1999) 1648;
(d) M.V. Bennett, L.G. Beauvais, M.P. Shores, J.R. Long, J. Am. Chem. Soc. 123 (2001) 8022.
[6] (a) K.K. Klausmeyer, T.B. Rauchfuss, S.R. Wilson, Angew. Chem. Int. Ed. 37 (1998) 1694;
(b) A.M.A. Ibrahim, Polyhedron 18 (1999) 2111.
[7] D.J. Darensbourg, A.L. Phelps, Inorg. Chim. Acta 357 (2004) 1603.
[8] (a) T. Mallah, S. Thiebault, M. Verdaguer, P. Veillet, Science 262 (1993) 1554;
(b) S. Ferlay, T. Mallah, R. Ouahes, P. Veillet, M. Verdaguer, Nature (London) 378 (1995) 701;
(c) R. Garde, F. Villain, M. Verdaguer, J. Am. Chem. Soc. 124 (2002) 10531;
(d) W.R. Entley, G.S. Girolami, Science 268 (1995) 397;
(e) S.M. Holmes, G.S. Girolami, J. Am. Chem. Soc. 121 (1999) 5593;
(f) W.E. Hatlevik, J. Buschmann, J.L. Zhang, J.S. Manson, Miller. Adv. Mater. 11 (1999) 914.
[9] (a) O. Sato, T. Iyoda, A. Fujishima, K. Hashimoto, Science 271 (1996) 49;
(b) O. Sato, S. Hayami, Y. Einaga, Z.Z. Gu, Bull. Chem. Soc. Jpn. 76 (2003) 443.
[10] (a) O. Sato, T. Iyoda, A. Fujishima, K. Hashimoto, Science 272 (1996) 704;
(b) S. Ohkoshi, M. Mizuno, G. Hung, K. Hashimoto, J. Phys. Chem. B 104 (2000) 8365.
[11] M. Mizuno, S. Ohkoshi, K. Hashimoto, Adv. Mater. 12 (2000) 1855.
[12] (a) S. Gatteschi, R. Sessoli, Angew. Chem. Int. Ed. 42 (2003) 268;
(b) J.N. Rebilly, T. Mallah, Struct. Bonding (Berlin) 122 (2006) 103.
[13] R. Lescouezec, L.M. Toma, J. Vaissermann, M. Verdaguer, F.S. Delgado, C. Ruiz-Perez, F. Lloret, M. Julve, Coord. Chem. Rev. 249 (2005) 2691.
[14] C. Coulon, H. Miyasaka, R. Clérac, Struct. Bonding (Berlin) 122 (2006) 163.
[15] H.L. Sun, Z.M. Wang, S. Gao, Coord. Chem. Rev. 254 (2009) 1081.
[16] H. Miyasaka, M. Julve, M. Yamashita, Inorg. Chem. 48 (2009) 3420.
[17] E.D. Dahlberg, J.G. Zhu, Phys. Today (1995) 34.
[18] G.P. Berman, G.D. Doolen, D.D. Holm, V.I. Tsifrinovich, Phys. Lett. A 193 (1994) 444.
[19] D.A. Garanin, E.M. Chudnovsky, Phys. Rev. B 56 (1997) 11102.
[20] H. Weihe, H.U. Güdel, Comments Inorg. Chem. 22 (2000) 75.
[21] (a) V. Marvaud, C. Decroix, A. Scuiller, C. Guyard-Duhayon, J. Vaissermann, F. Gonnet, M. Verdaguer, Chem. Eur. J. 9 (2003) 1678;
(b) V. Marvaud, C. Decroix, A. Scuiller, F. Tuyeras, C. Guyard-Duhayon, J. Vaissermann, J. Marrot, F. Gonnet, M. Verdaguer, Chem. Eur. J. 9 (2003) 1692.
[22] (a) T. Mallah, C. Auberger, M. Verdaguer, P. Veillet, Chem. Commun. (1995) 61;
(b) R.J. Parker, D.C.R. Hockless, B. Moubaraki, K.S. Murray, L. Spiccia, Chem. Commun. (1996) 2789.
[23] L.M.C. Beltran, J.R. Long, Acc. Chem. Res. 38 (2005) 325.
[24] L.M. Toma, L.D. Toma, F.S. Delgado, C. Ruiz-Perez, J. Sletten, J. Cano, J.M. Clemente-Juan, F. Lloret, M. Julve, Coord. Chem. Rev. 250 (2006) 2176.
[25] J.L. Boyer, M.L. Kuhlman, T.B. Rauchfuss, Acc. Chem. Res. 40 (2007) 233.
[26] R. Lescouëzec, J. Vaissermann, F. Lloret, M. Julve, M. Verdaguer, Inorg. Chem. 41 (2002) 5943.
[27] D.f. Li, S. Parkin, G. Wang, G.T. Yee, S.M. Holmes, Inorg. Chem. 45 (2006) 1951.
[28] D.f. Li, R. Clérac, S. Parkin, G. Wang, G.T. Yee, S.M. Holmes, Inorg. Chem. 45 (2006) 5251.
[29] C.F. Wang, W. Liu, Y. Song, X.H. Zhou, J.L. Zuo, X.Z. You, Eur. J. Inorg. Chem. (2008) 717.
[30] T.D. Harris, J.R. Long, Chem. Commun. (2007) 1360.
[31] D.f. Li, S. Parkin, G. Wang, G.T. Yee, S.M. Holmes, Inorg. Chem. 45 (2006) 2773.
[32] R. Lescouezec, J. Vaissermann, L.M. Toma, R. Carrasco, F. Lloret, M. Julve, Inorg. Chem. 43 (2004) 2234.
[33] J. Il Kim, H.S. Yoo, E.K. Koh, H.C. Kim, C.S. Hong, Inorg. Chem. 46 (2007) 8481.
[34] J. Il Kim, H.S. Yoo, E.K. Koh, C.S. Hong, Inorg. Chem. 46 (2007) 10461.
[35] L.M. Toma, D. Armentano, G.D. Munno, J. Sletten, F. Lloret, M. Julve, Polyhedron 26 (2007) 5263.
[36] J. Il Kim, H.Y. Kwak, J.H. Yoon, D.W. Ryu, I.Y. Yoo, N. Yang, B.K. Cho, J.G. Park, H. Lee, C.S. Hong, Inorg. Chem. 48 (2009) 2956.
[37] M. Goto, N. Koga, Y. Ohse, Y. Kudoh, M. Kukihara, Y. Okuno, H. Kurosaki, Inorg. Chem. 43 (2004) 5120.
[38] Z.G. Gu, J.L. Zuo, Y. Song, C.H. Li, Y.Z. Li, X.Z. You, Inorg. Chem. Acta 358 (2005) 4057.
[39] J. Il Kim, J.H. Yoon, E.K. Koh, C.S. Hong, Eur. J. Inorg. Chem. (2008) 2756.
[40] J.Q. Tao, T.W. Wang, Z.G. Gu, J.L. Zuo, X.Z. You, Chin. J. Inorg. Chem. 22 (2006) 2207.
[41] D.Y. Wu, O. Sato, Z. Anorg. Allg. Chem. 635 (2009) 389.
[42] J. Wei, X.Q. Liang, Y.Z. Li, J.L. Zuo, X.Z. You, Chin. J. Inorg. Chem. 23 (2007) 473.
[43] H.Y. Kwak, D.W. Ryu, H.C. Kim, E.K. Koh, B.K. Cho, C.S. Hong, Inorg. Chem. 49 (2010) 4632.
[44] S. Wang, J.L. Zuo, H.C. Zhou, Y. Song, S. Gao, X.Z. You, Eur. J. Inorg. Chem. (2004) 3681.

[45] J. Kim, S. Han, I.K. Cho, K.Y. Choi, M. Heu, S. Yoon, B.J. Suh, Polyhedron 23 (2004) 1333.
[46] S. Wang, J.L. Zuo, H.C. Zhou, Y. Song, X.Z. You, Inorg. Chim. Acta 358 (2005) 2101.
[47] J.Z. Gu, L. Jiang, J.H. Liang, T.B. Lu, M.Y. Tan, Chin. J. Inorg. Chem. 22 (2006) 1375.
[48] H.R. Wen, C.F. Wang, J.L. Zuo, Y. Song, X.R. Zeng, X.Z. You, Inorg. Chem. 45 (2006) 582.
[49] Z.H. Ni, H.Z. Kou, L.F. Zhang, W.W. Ni, Y.B. Jiang, A.L. Cui, J. Ribas, O. Sato, Inorg. Chem. 44 (2005) 9631.
[50] C.F. Wang, Z.G. Gu, X.M. Lu, J.L. Zuo, X.Z. You, Inorg. Chem. 47 (2008) 7957.
[51] J.Z. Gu, L. Jiang, M.Y. Tan, T.B. Lu, J. Mol. Struct. 890 (2008) 24.
[52] M. Nihei, M. Ui, H. Oshio, Polyhedron 28 (2009) 1718.
[53] D.f. Li, S. Parkin, G. Wang, G.T. Yee, A.V. Prosvirin, S.M. Holmes, Inorg. Chem. 44 (2005) 4903.
[54] W. Liu, C.F. Wang, Y.Z. Li, J.L. Zuo, X.Z. You, Inorg. Chem. 45 (2006) 10058.
[55] D.F. Li, R. Clérac, G.B. Wang, G.T. Yee, S.M. Holmes, Eur. J. Inorg. Chem. (2007) 1341.
[56] D.Y. Wu, Y.J. Zhang, W. Huang, O. Sato, Dalton Trans. (2010) 5500.
[57] C.F. Wang, J.L. Zuo, J.W. Ying, T. Ren, X.Z. You, Inorg. Chem. 47 (2008) 9716.
[58] H.Y. Kwak, D.W. Ryu, H.C. Kim, E.K. Koh, B.K. Cho, C.S. Hong, Dalton Trans. (2009) 1954.
[59] Z.G. Gu, Q.F. Yang, W. Liu, Y. Song, Y.Z. Li, J.L. Zuo, X.Z. You, Inorg. Chem. 45 (2006) 8895.
[60] C.F. Wang, J.L. Zuo, B.M. Bartlett, Y. Song, J.R. Long, X.Z. You, J. Am. Chem. Soc. 128 (2006) 7162.
[61] Z.G. Gu, W. Liu, Q.F. Yang, X.H. Zhou, J.L. Zuo, X.Z. You, Inorg. Chem. 46 (2007) 3236.
[62] B.M. Bartlett, T.D. Harris, M.W. DeGroot, J.R. Long, Z. Anorg. Allg. Chem. 633 (2007) 2380.
[63] J. Kim, S. Han, K.I. Pokhodnya, J.M. Migliori, J.S. Miller, Inorg. Chem. 44 (2005) 6983.
[64] Y.J. Zhang, T. Liu, S. Kanegawa, O. Sato, J. Am. Chem. Soc. 131 (2009) 7942.
[65] D.f. Li, S. Parkin, G. Wang, G.T. Yee, R. Clérac, W. Wernsdorfer, S.M. Holmes, J. Am. Chem. Soc. 128 (2006) 4214.
[66] D.F. Li, S. Parkin, R. Clérac, S.M. Holmes, Inorg. Chem. 45 (2006) 7569.
[67] D.F. Li, R. Clérac, O. Roubeau, E. Harté, C. Mathonière, R.L. Bris, S.M. Holmes, J. Am. Chem. Soc. 130 (2008) 252.
[68] M. Nihei, M. Ui, N. Hoshino, H. Oshio, Inorg. Chem. 47 (2008) 6106.
[69] C.C. Shi, C.S. Chen, S.C.N. Hsu, W.Y. Yeh, M.Y. Chiang, T.S. Kuo, Inorg. Chem. Commun. 11 (2008) 1264.
[70] Y. Zhang, U.P. Mallik, N. Rath, G.T. Yee, R. Clérac, S.M. Holmes, Chem. Commun. 46 (2010) 4953.
[71] S. Wang, J.L. Zuo, H.C. Zhou, H.J. Choi, Y. Ke, J.R. Long, X.Z. You, Angew. Chem. Int. Ed. 43 (2004) 5940.
[72] L. Jiang, H.J. Choi, X.L. Feng, T.B. Lu, J.R. Long, Inorg. Chem. 46 (2007) 2181.
[73] S. Wang, J.L. Zuo, S. Gao, Y. Song, H.C. Zhou, Y.Z. Zhang, X.Z. You, J. Am. Chem. Soc. 126 (2004) 8900.
[74] L. Jiang, X.L. Feng, T.B. Lu, S. Gao, Inorg. Chem. 45 (2006) 5018.
[75] K. Mitsumoto, M. Ui, M. Nihei, H. Nishikawa, H. Oshio, Crystengcomm 12 (2010) 2697.
[76] Z.G. Gu, J.L. Zuo, Y. Song, C.H. Li, Y.Z. Li, X.Z. You, Inorg. Chim. Acta 358 (2005) 4057.
[77] S. Wang, M. Ferbinteanu, M. Yamashita, Inorg. Chem. 46 (2007) 610.
[78] S. Wang, M. Ferbinteanu, M. Yamashita, Solid State Sci. 10 (2008) 915.
[79] V. Costa, R. Lescouëzec, J. Vaissermann, P. Herson, Y. Journaux, M.H. Araujo, J.M. Clemente-Juan, F. Lloret, M. Julve, Inorg. Chim. Acta 361 (2008) 3912.